Modal Control of a Satellite in an Unstable Periodic Orbit About the Earth-Sun Interior Lagrange Point

THESIS

Douglas J Hopper
First Lieutenant, USAF

AFIT/GA/ENY/93D-3

Approved for public release; distribution unlimited

The views expressed in this thesis are those of the author and do not reflect the official policy of position of the Department of Defense or the U. S. Government

AFIT/GA/ENY/93D-3

Modal Control of a Satellite in an Unstable Periodic Orbit About the Earth-Sun Interior Lagrange Point

THESIS

Presented to the Faculty of the Graduate School of Engineering
of the Air Force Institute of Technology
Air University
In Partial Fulfillment of the
Requirements for the Degree of
Master of Science in Astronautical Engineering

Douglas J Hopper, B.S. Mechanical Engineering
First Lieutenant, USAF

December, 1993

Preface

On August 28, 1978, the first artificial satellite was launched into an unstable periodic orbit about the interior libration point (or Lagrange point) between the sun and the earth. It was called International Sun-Earth Explorer, ISEE-3, and its purpose was to make accurate measurements of the magnetic phenomena in the solar wind. Proposed by Farquhar (2), it was our first libration point satellite, demonstrating what Floquet, Poincaré and Lagrange could only think, write and dream about.

Other missions using similar orbits have been proposed, and the purpose of this thesis is to discuss the control of satellites in such an orbit using Floquet theory.

Douglas J Hopper

Table of Contents

		Page
Preface		ii
List of Figures		v
Abstract		viii
I.	Introduction	1-1
II.	Background	2-1
	2.1 Restricted Three Body Problem	2-1
	2.2 Periodic Orbits	2-5
	2.3 The Halo Orbit	2-6
	2.4 Floquet Theory	2-7
	2.5 Extended Eigenvectors	2-12
	2.6 Results of the Eigenvalue-Eigenvector Problem	2-14
	2.7 Summary	2-15
III.	Theory	3-1
	3.1 Canonical Transformations	3-1
	3.2 Fourier Representations	3-2
IV.	Controllers	4-1
	4.1 The Halo Orbit	4-1
	4.2 The "Cheater" Controller	4-1
	4.3 Maneuver Optimisation	4-3
	4.4 Results of the Realistic Controller	4-8
	4.5 Optimisation of Maneuver Epoch	4-19

Page

4.6 Behavior of the Other Modes 4-24

4.7 Summary 4-27

V. Perturbations 5-1

5.1 The Perturbed System 5-1

5.2 The Elliptic Restricted Problem 5-4

5.3 The Elliptic Four Body Problem 5-8

VI. Results of Perturbation Controller 6-1

6.1 Simplification of System 6-1

6.2 Results 6-4

6.3 Behavior of the Other Modes 6-14

6.4 Summary 6-14

VII. Conclusions and Recommendations 7-1

7.1 Conclusions 7-1

7.2 Recommendations 7-2

Bibliography BIB-1

Vita VITA-1

List of Figures

Figure		Page
2.1.	The Three Dimensional Restricted Three-Body Problem	2-2
2.2.	Four Representations of Halo Orbit	2-8
4.1.	X — Y Projection of Orbit Showing that the Satellite does not Remain Close to the Nominal Orbit. The Earth is at About X = -1, Y = 0.	4-2
4.2.	Oscillatory Modes Plotted Against One Another for 99 Periods .	4-4
4.3.	Average Maneuver Cost as a Function of Time (Canonical Units), Threshold = 10^{-7}	4-9
4.4.	Average Maneuver Cost as a Function of Time (Canonical Units), Threshold = 10^{-9}	4-10
4.5.	Plot of the Two Real Modes as the Realistic Controller Operates, Threshold = 10^{-7}	4-11
4.6.	Close-Up of the Two Real Modes for 100 Time Units as the First Realistic Controller Operates Showing the Saddle Behavior, Threshold = 10^{-7}	4-13
4.7.	Plot of the Two Real Modes as the Realistic Controller Operates Showing the Saddle Behavior, Threshold = 10^{-9}	4-14
4.8.	Average Maneuver Cost as a Function of Time, Threshold = 10^{-3}	4-15
4.9.	Plot of the Real Modes for an Insufficient Amount of Control, Threshold = 10^{-3}, Showing Nonlinear Behavior of the Modes . .	4-16
4.10.	Plot of the Y – Z Projection of the Orbit, Threshold = 10^{-3}, Showing that the Orbit Changes Radically While Remaining in Vicinity of L_2 (Origin)	4-17
4.11.	Performance of the Realistic Controller as a Function of the Controller's Threshold Value	4-18
4.12.	Plot of λ Versus Time for 3.3 Periods Showing its Periodic Nature with Minima Occurring Once per Orbit	4-21

Figure Page

4.13. Average Maneuver Cost as a Function of Time While Maneuvering Once per Orbit at the Optimal Time 4-22

4.14. X – Y Projection Plot of the Maneuvering Portion of the Halo Orbit Under Periodic Control 4-23

4.15. Imaginary Modes Plotted Together While Satellite is Under Realistic Control 4-25

4.16. Zero Modes Plotted Together While Satellite is Under Realistic Control 4-26

5.1. The Elliptic Restricted Problem 5-5

5.2. Frame of Reference for the Restricted Four Body Problem 5-9

5.3. More Detail on the Restricted Four Body Problem 5-10

6.1. X – Y Projection of Satellite Path Diverging Before Completing First Orbit. (.... = Periodic Orbit — = Satellite Path) 6-2

6.2. X – Y Projection of Satellite Path Diverging Even Without Eccentricity. (.... = Periodic Orbit — = Satellite Path) 6-3

6.3. Average Station-Keeping Cost for Moon-Perturbed Orbit, Threshold = 10^{-3} 6-4

6.4. Plot of the Real Modes, Threshold = 10^{-3} 6-5

6.5. Plot of the Y – Z Projection of the Orbit, Threshold = 10^{-3} . . . 6-6

6.6. Station-Keeping Cost with Threshold = 10^{-6} Showing the Maneuvering is Extremely Frequent. 6-7

6.7. Y – Z Projection (Like the View from Earth) of Controlled Satellite's Orbit, Threshold = 10^{-6} 6-8

6.8. Station-Keeping Cost, Threshold = 2×10^{-5} 6-9

6.9. Real Modes Under Control for Threshold = 2×10^{-5} 6-10

6.10. Y – Z Projection for the Satellite Path, Threshold = 2×10^{-5} . . 6-11

6.11. Station-Keeping Cost as a Function of Threshold 6-12

6.12. Cost Comparison for Perturbed (+) vs Unperturbed (o) Systems 6-13

Figure Page

6.13. Imaginary Modes Plotted Together While Satellite is Under Realistic Control 6-15

6.14. Zero Modes Plotted Together While Satellite is Under Realistic Control 6-16

Abstract

A periodic "halo" orbit which exists about the interior Lagrange point for the Earth-sun system was decomposed using Floquet theory into modal variables, which are dynamically decoupled subspaces for the six degree of freedom system. Modal control consisted of evaluating the diverging mode and maneuvering to counteract its divergence. In the unperturbed system this was successful. Control costs were low, and the significance is that the controller did nothing to suppress modes that were oscillatory or converging. First order perturbations by the moon and Earth's eccentricity were examined. The effect of the moon's motion allowed the scheme to operate with reasonable control costs, but the effect of eccentricity caused divergence in spite of the controller.

Modal Control of a Satellite in an Unstable Periodic Orbit About the Earth-Sun Interior Lagrange Point

I. Introduction

It is desirable to have a satellite upstream of the Earth to study the solar wind and to warn us of variations in solar activity. The mathematics of the restricted three-body problem predict an equilibrium point in the space between Earth and the sun. Ideally, a satellite placed at this point could literally remain there indefinitely. However, a satellite at the interior Lagrange point (or L_2) is directly between earth and sun, so from any observation station on Earth, it would appear in the center of the sun's disk. This is a poor place from which to receive the very low-power transmissions necessary for data reception and tracking. We can, however, orbit a satellite about the Lagrange point, as was successfully demonstrated in 1978 with ISEE-3 (6). If a simple periodic orbit can be found, it is called a Halo orbit. L_2 is an unstable libration point in the three-body problem (8: 271) and the halo orbit in the vicinity of L_2 that we used for this study is also unstable. Any satellite placed into such an orbit would require station-keeping. Without some control input over time, a satellite placed near such an orbit will not remain near, but quickly wander off into space surprisingly far from the intended path. Even if we could inject a satellite exactly *into* a halo orbit and not just *near* one, it would not remain there indefinitely since the universe we live in is not completely described by the restricted three-body problem. This is analogous to trying to balance a pencil indefinitely on its point. Even if you placed it perfectly in balance and there were no wind or vibrations, eventually some ridiculously small force such as the coriolis effect or the moon's gravity would knock it over. This paper will concentrate on the instabilities

inherent in the orbit and the perturbing effects of the Earth's eccentricity and the moon.

The station-keeping of ISEE-3 was accomplished by calculation of a nominal periodic orbit, a reference orbit, from which it was allowed to stray only a certain amount before its small thrusters were fired to kick it back closer to the reference orbit. There may be a better way. In this paper we will use the theory of Floquet to demonstrate that while the orbit is unstable, only one of its six Floquet modes is unstable. It is our goal to suppress only this mode, while leaving the stable modes and the oscillatory modes to their own devices. The stable modes will tend to bring the satellite closer to the reference orbit in the long run, even if the orbit itself appears to be diverging at any given time, and likewise, the oscillatory modes will not diverge, but wobble back and forth across the nominal trajectory. Modal control is not a new concept. Wiesel and Shelton (11) proposed a modal control algorithm in 1983 to control a satellite in an orbit about the exterior Earth-Moon Lagrange point (L_1). This study differs from theirs in that we will use impulsive maneuvers to control the satellite instead of the continuous low-thrust control they proposed.

In order to lead up to the problem, Chapter II will explain the dynamics of the restricted three-body problem, which is a Hamiltonian system. It is that problem on which we will use the theory of Floquet. The modes will be found and explained, and then a controller will be devised using impulsive thrusters. A maneuver is performed when the unstable mode grows beyond a certain limit — the "threshold". The direction of the maneuver is determined by the projection of the unstable mode onto the three momentum states. We will run simulations to verify that the control action worked and evaluate the control energy expended. We will then add perturbations due to the moon and the eccentricity of Earth's orbit. Simulations will be run to see what effects these perturbations have and if the controller still works.

II. Background

The satellite we wish to control is not in orbit about the earth, nor is it entirely in an orbit about the sun. It is in what is called a ***three-body orbit*** where the satellite is the third body in orbit about the other two (called ***primaries***, or the primary and secondary bodies). The three-body problem is an old one, having been studied by Euler, Lagrange and others as early as 1772 (see (7: 4)). We will describe the "restricted three-body problem" and find equations of motion.

2.1 Restricted Three Body Problem

Imagine two massive bodies, each under the gravitational influence of the other, rotating about their common center of mass in circular orbits. A third body, assumed to have negligible mass — it does not affect the motion of the primary and secondary bodies — orbits under the influence of both. Its motion is affected only by the two primaries. The description of the motion of this third body is the solution to the restricted three-body problem (7: 8).

The earth and sun with a satellite at relatively large distance from either is an example of a system for which the restricted three-body problem (RTBP or three-body problem) is a good first approximation. The sun is the primary (designated m_1), the earth-moon system is the secondary, m_2, and the units are chosen so that the sum of their masses, the distance between them, and the gravitational constant are all unity. This leads to the fact that the angular frequency, ω, of their motion (and therefore our rotating reference frame) is unity as well (see figure 2.1).

Defining the parameter $\mu = m_2$, we have $m_1 = 1 - \mu$ and the center of mass of the system (remember that the third body has negligible mass) is found to be a distance μ from m_1 leaving $1 - \mu$ between center and m_2. We set our origin at the center of mass, with the positive x axis pointing toward m_1. The z axis points

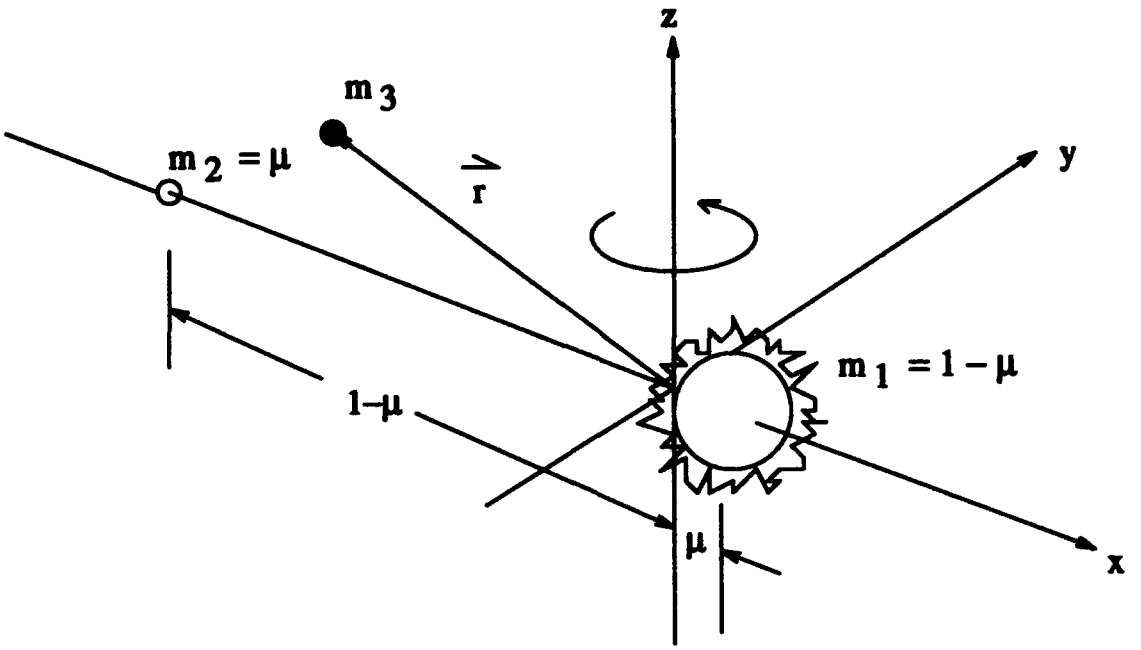

Figure 2.1. The Three Dimensional Restricted Three-Body Problem

upward, and the y axis completes a right-handed coordinate system. The frame rotates with $\vec{\omega} = 1\hat{k}$.

The third body, m_3, the reference satellite, has position vector, $\vec{r} = x\hat{\imath} + y\hat{\jmath} + z\hat{k}$ in rectangular coordinates. Differentiating with respect to time, we obtain

$$\begin{aligned} \dot{\vec{r}} &= \dot{x}\hat{\imath} + \dot{y}\hat{\jmath} + \dot{z}\hat{k} + \vec{\omega} \times \vec{r} \\ &= (\dot{x} - y)\hat{\imath} + (\dot{y} + x)\hat{\jmath} + \dot{z}\hat{k}. \end{aligned} \tag{2.1}$$

The kinetic energy per unit mass is

$$\begin{aligned} T &= \tfrac{1}{2}\dot{\vec{r}} \cdot \dot{\vec{r}} \\ &= \tfrac{1}{2}\left[(\dot{x} - y)^2 + (\dot{y} + x)^2 + \dot{z}^2\right]. \end{aligned} \tag{2.2}$$

The potential energy per unit mass is

$$V = -G\left(\frac{m_1}{\rho_1} + \frac{m_2}{\rho_2}\right) \tag{2.3}$$

where

$$\rho_1 = \sqrt{(x-\mu)^2 + y^2 + z^2} \tag{2.4}$$

and

$$\rho_2 = \sqrt{(x-\mu+1)^2 + y^2 + z^2}. \tag{2.5}$$

But, remembering that G is equal to one in our chosen units, and substituting the parameter μ for the masses,

$$V = \left[\frac{1-\mu}{\rho_1} + \frac{\mu}{\rho_2}\right]. \tag{2.6}$$

The Lagrangian for this system is

$$\begin{aligned} L &= T - V & (2.7)\\ &= \frac{1}{2}\left[(\dot{x}-y)^2 + (\dot{y}+x)^2 + \dot{z}^2\right] - \left[\frac{1-\mu}{\rho_1} + \frac{\mu}{\rho_2}\right]. & (2.8) \end{aligned}$$

Now from the definition of generalized momenta, $p_k = \dfrac{\partial L}{\partial \dot{q}_k}$, we have

$$\begin{aligned} p_x &= \frac{\partial L}{\partial \dot{x}} = \dot{x} - y, & (2.9)\\ p_y &= \frac{\partial L}{\partial \dot{y}} = \dot{y} + x, & (2.10)\\ p_z &= \frac{\partial L}{\partial \dot{z}} = \dot{z}, & (2.11) \end{aligned}$$

and we see by comparing equations 2.9–2.11 to equation 2.1 that the generalized momenta are the components of the inertial velocity vector.

The definition of the Hamiltonian, $H = \sum_{k=1}^{n} p_k \dot{q}_k - L$ after eliminating $\dot{q}_k$'s in favor of p_k's, yields:

$$H = \frac{1}{2}(p_x^2 + p_y^2 + p_z^2) + p_x y - p_y x - \left[\frac{(1-\mu)}{\rho_1} + \frac{\mu}{\rho_2}\right]. \tag{2.12}$$

Hamilton's equations of motion are given by

$$\dot{q}_k = \frac{\partial H}{\partial p_k}, \quad \dot{p}_k = -\frac{\partial H}{\partial q_k}, \tag{2.13}$$

so performing the necessary partial differentiation leads to the equations of motion

$$\dot{x} = p_x + y \tag{2.14}$$

$$\dot{y} = p_y - x \tag{2.15}$$

$$\dot{z} = p_z \tag{2.16}$$

$$\dot{p}_x = p_y + \left[\frac{(1-\mu)(x-\mu)}{\rho_1^3} + \frac{\mu(x-\mu+1)}{\rho_2^3}\right] \tag{2.17}$$

$$\dot{p}_y = -p_x + \left[\frac{(1-\mu)y}{\rho_1^3} + \frac{\mu y}{\rho_2^3}\right] \tag{2.18}$$

$$\dot{p}_z = \left[\frac{(1-\mu)z}{\rho_1^3} + \frac{\mu z}{\rho_2^3}\right]. \tag{2.19}$$

Now let the state vector for the system be defined by

$$X^T = (x, y, z, p_x, p_y, p_z) \tag{2.20}$$

then

$$\dot{X}^T = (\dot{x}, \dot{y}, \dot{z}, \dot{p}_x, \dot{p}_y, \dot{p}_z). \tag{2.21}$$

Introduce the matrix Z, which is defined by

$$Z = \begin{pmatrix} 0 & I_3 \\ -I_3 & 0 \end{pmatrix} \tag{2.22}$$

where I_3 is a 3×3 identity matrix and 0 represents a 3×3 null matrix. Then we can write

$$\dot{X} = Z\frac{\partial H}{\partial X} \tag{2.23}$$

which is a restatement of Hamilton's equations of motion in state vector form. This formulation is general in that it can be used for any Hamiltonian system.

2.2 Periodic Orbits

The third body in our problem is in orbit about the primaries. We would like to find out what its orbit looks like in order to predict and control the state of the satellite. If this were the two-body problem, the answer would be quite simple. All two-body orbits are conic sections: ellipses for relatively low energy orbits, hyperbolas for the high energy orbits, with parabolic orbits as the limiting case in between. All elliptic two-body orbits are planar and *periodic*. Given a period of τ, the state vector at time $\tau + t_0$ is identical to the state vector at time t_0.

Not all the orbits in the three-body problem are periodic, but periodic orbits do exist. They are interesting because we can make predictions about the behavior of periodic orbits over long periods of time that cannot be made about non-periodic orbits. Finding a periodic orbit is a matter of guessing initial conditions to the state vector and then integrating the equations of motion through one period. The difference between the initial state vector and the final state vector is the error, $e = x(\tau) - x(0)$. The initial conditions (and the period if necessary) are then adjusted until the error vanishes. In order to make corrections to the initial conditions, the matrix, $\Phi(\tau, 0)$, needs to be found. Φ is the differential state transition matrix, which relates *small* changes in the state according to

$$\delta x(t) = \Phi(t, t_0) X(t_0) \tag{2.24}$$

where $\delta x = X(t) - X(t_0)$. This is a linear equation. It is only valid in a region of the phase space where $X(t)$ is relatively close to $X(t_0)$, as it will be if $t = \tau$ and $t_0 = 0$ and provided we have chosen a set of initial conditions near a periodic orbit. Φ is found from the variational equations of the system, introduced in section 2.4.

2.3 *The Halo Orbit*

To find the orbit for this study we first found the value for the dimensionless parameter, μ. Let $m_1 = m_\odot$, the mass of the sun, and $m_2 = m_\oplus + m_\varnothing$, the sum of the masses of Earth and the moon, respectively. With a little algebra, it can be seen that

$$\mu = \frac{m_2}{m_1 + m_2} \tag{2.25}$$

so we obtain

$$\mu = \frac{m_\oplus + m_\varnothing}{m_\odot + m_\oplus + m_\varnothing} = 3.040357143 \times 10^{-6}. \tag{2.26}$$

Next, we looked at the orbit from ISEE-3. Richardson (6) gave approximate values for that orbit. We transformed the approximate initial conditions into our own reference frame (see figure 2.1) and were able to converge to a periodic orbit by iteratively correcting those initial conditions. The initial conditions we converged on were

$$X(t_0) = \left\{ \begin{array}{l} -.9916251451934399 \\ 0.0 \\ -.0006706478525000000 \\ 0.0 \\ -.9818296716854701 \\ 0.0 \end{array} \right\} \tag{2.27}$$

These are neither exact nor unique. Any point on (or very near) the periodic orbit could be used as initial conditions, and will yield the same trajectory. The period was found to be

$$\tau = 3.0596432056926\ TU \tag{2.28}$$

given in canonical time units (described below), or about 177.86 days. The first three elements of the state vector (x, y and z) are in distance units and the last three (p_x, p_y and p_z) are in distance units per time unit. A distance unit in this problem is an Astronomical Unit (AU) which is approximately 1.495978×10^8 kilometers. A time

unit is $\frac{1}{2\pi}$ times the period of the rotating reference frame. Since that period is one year for this system, one time unit is about 2 months (58.132356144 days). These are referred to as *canonical* units. Referring to figure 2.1 for the reference frame, we see that the initial conditions place the satellite about one hundredth of the way to the sun from Earth, slightly below the ecliptic plane. Since the orbit is not planar, visualisation can be a rather difficult problem. Figure 2.2 shows the projections of the orbit onto the principle (X-Y, Y-Z, and X-Z) planes and a "three-dimensional" view as well.

This orbit is hereafter referred to as the periodic orbit and is the reference orbit used in this study.

2.4 Floquet Theory

A periodic orbit is a special solution to the equations of motion for the system, just as an equilibrium point is a solution. There are many problems that have been solved by linearising equations of motion about an equilibrium point to obtain a constant coefficient linear system, and in much the same way, we linearise about a periodic orbit to obtain a time periodic linear system. A Hamiltonian system is linearized by taking the partial derivative of the equations of motion with respect to the state vector.

$$\frac{\partial \dot{X}}{\partial X} = Z\frac{\partial^2 H}{\partial X^2} \tag{2.29}$$

We define $A(t)$ as the matrix of second partial derivatives.

$$A(t) = Z\frac{\partial^2 H}{\partial X^2} \tag{2.30}$$

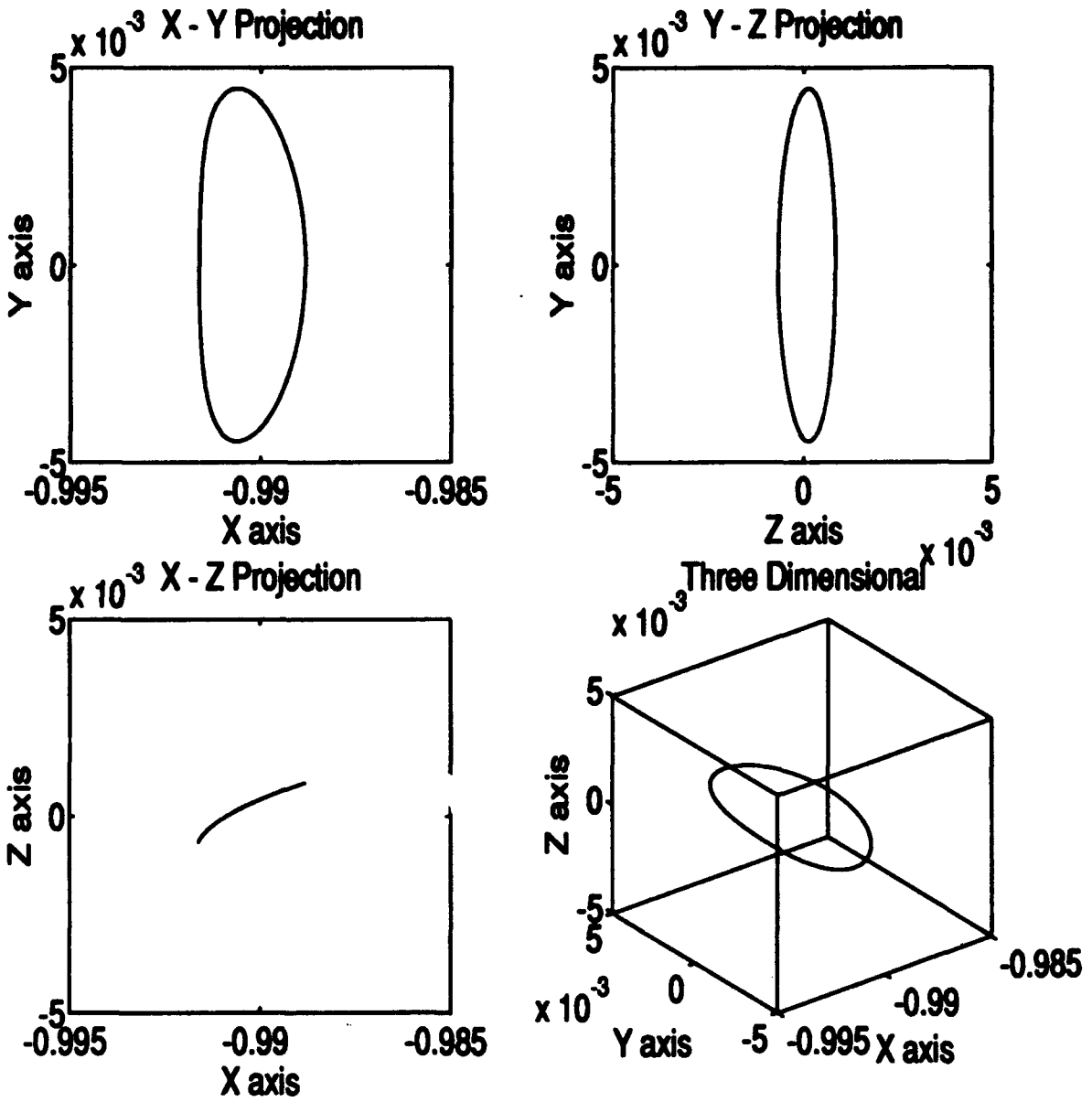

Figure 2.2. Four Representations of Halo Orbit

The left side of Eq. 2.29 then becomes

$$\begin{Bmatrix} \frac{\partial \dot{x}}{\partial x} & \frac{\partial \dot{x}}{\partial y} & \frac{\partial \dot{x}}{\partial z} & \frac{\partial \dot{x}}{\partial p_x} & \frac{\partial \dot{x}}{\partial p_y} & \frac{\partial \dot{x}}{\partial p_z} \\ \frac{\partial \dot{y}}{\partial x} & \frac{\partial \dot{y}}{\partial y} & \frac{\partial \dot{y}}{\partial z} & \frac{\partial \dot{y}}{\partial p_x} & \frac{\partial \dot{y}}{\partial p_y} & \frac{\partial \dot{y}}{\partial p_z} \\ \frac{\partial \dot{z}}{\partial x} & \frac{\partial \dot{z}}{\partial y} & \frac{\partial \dot{z}}{\partial z} & \frac{\partial \dot{z}}{\partial p_x} & \frac{\partial \dot{z}}{\partial p_y} & \frac{\partial \dot{z}}{\partial p_z} \\ \frac{\partial \dot{p}_x}{\partial x} & \frac{\partial \dot{p}_x}{\partial y} & \frac{\partial \dot{p}_x}{\partial z} & \frac{\partial \dot{p}_x}{\partial p_x} & \frac{\partial \dot{p}_x}{\partial p_y} & \frac{\partial \dot{p}_x}{\partial p_z} \\ \frac{\partial \dot{p}_y}{\partial x} & \frac{\partial \dot{p}_y}{\partial y} & \frac{\partial \dot{p}_y}{\partial z} & \frac{\partial \dot{p}_y}{\partial p_x} & \frac{\partial \dot{p}_y}{\partial p_y} & \frac{\partial \dot{p}_y}{\partial p_z} \\ \frac{\partial \dot{p}_z}{\partial x} & \frac{\partial \dot{p}_z}{\partial y} & \frac{\partial \dot{p}_z}{\partial z} & \frac{\partial \dot{p}_z}{\partial p_x} & \frac{\partial \dot{p}_z}{\partial p_y} & \frac{\partial \dot{p}_z}{\partial p_z} \end{Bmatrix} \tag{2.31}$$

and when the partial derivatives are taken for the RTBP in question, A(t) is given by

$$A(t) = \begin{Bmatrix} 0 & 1 & 0 & 1 & 0 & 0 \\ -1 & 0 & 0 & 0 & 1 & 0 \\ 0 & 0 & 0 & 0 & 0 & 1 \\ A_{41} & A_{42} & A_{43} & 0 & 1 & 0 \\ A_{51} & A_{52} & A_{53} & -1 & 0 & 0 \\ A_{61} & A_{62} & A_{63} & 0 & 0 & 0 \end{Bmatrix} \tag{2.32}$$

where

$$
\begin{aligned}
A_{41} &= 1 - \frac{1-\mu}{\rho_1^3} + \frac{3(1-\mu)(x-\mu)^2}{\rho_1^5} - \frac{\mu}{\rho_2^3} + \frac{3\mu(x+1-\mu)^2}{\rho_2^5} \\
A_{42} &= A_{51} = -\frac{3y(x-\mu)(1-\mu)}{\rho_1^5} - \frac{3y\mu(x-\mu+1)}{\rho_2^5} \\
A_{43} &= A_{61} = -\frac{3z(x-\mu)(1-\mu)}{\rho_1^5} - \frac{3z\mu(x-\mu+1)}{\rho_2^5} \\
A_{52} &= 1 - \frac{1-\mu}{\rho_1^3} + \frac{3(1-\mu)y^2}{\rho_1^5} - \frac{\mu}{\rho_2^3} + \frac{3\mu y^2}{\rho_2^5} \\
A_{53} &= A_{62} = -\frac{3yz(1-\mu)}{\rho_1^5} - \frac{3yz\mu}{\rho_2^5} \\
A_{63} &= -\frac{1-\mu}{\rho_1^3} + \frac{3(1-\mu)z^2}{\rho_1^5} - \frac{\mu}{\rho_2^3} + \frac{3\mu z^2}{\rho_2^5}
\end{aligned}
\tag{2.33}
$$

The linearisation of the equations of motion (2.23) takes the form

$$\delta\dot{x} = A(t)\delta x \tag{2.34}$$

Eq. 2.34 is called the variational equations for the system. The state transition matrix, $\Phi(t, t_0)$, also obeys

$$\dot{\Phi}(t, t_0) = A(t)\Phi(t, t_0) \tag{2.35}$$

By integrating Eqs. 2.23 and 2.35 (the equations of motion and the equations of variation) over one period we obtain $\Phi(\tau + t_0, t_0)$, the *monodromy matrix*. This is the Φ matrix used to find the orbit in section 2.3. Φ has no obviously meaningful structure, and it will not be given here, but its decomposition into eigenvalues and eigenvectors is given in section 2.6.

We learn from Floquet (9) that the solution to the variational equations can take the form of an eigenvalue-eigenvector problem

$$[\Phi(\tau + t_0, t_0) - \lambda_i I]\,\vec{f}_i = 0 \tag{2.36}$$

where λ_i are the eigenvalues and $\vec{f}_i$ are the corresponding eigenvectors of the monodromy matrix. The matrix of eigenvectors, F, will be important because it provides the transformation to our modal variables (see Chapter III). The Poincaré exponents, ω_i, are defined by $\omega_i = \frac{1}{\tau}\ln\lambda_i$, so the eigenvalues for $\Phi(\tau + t_0, t_0)$ can be expressed as $\lambda_i = e^{\omega_i \tau}$. The solution to this problem has traditionally been written as

$$\Phi(t, t_0) = F(t)e^{J(t-t_0)}F^{-1}(t_0) \tag{2.37}$$

where J is the (usually) diagonal matrix of Poincaré exponents, but this, of course, can only be done if the time periodic matrix, $F = (\vec{f}_1, \vec{f}_2, ...)$ is invertible. Assuming for now that it is invertible, we can differentiate Eq. 2.37 to get

$$\dot{\Phi}(t, t_0) = \dot{F}(t)e^{J(t-t_0)}F^{-1}(t_0) + F(t)Je^{J(t-t_0)}F^{-1}(t_0) \tag{2.38}$$

and substituting the right hand side of Eq. 2.35 into Eq. 2.38 and rearranging we get

$$\dot{F}e^{J(t-t_0)}F^{-1}(t_0) = A(t)F(t)e^{J(t-t_0)}F^{-1}(t_0) - F(t)Je^{J(t-t_0)}F^{-1}(t_0) \tag{2.39}$$

Noticing a common factor in Eq. 2.39 and dropping the notation for functional dependence on time, it simplifies to

$$\dot{F} = AF - FJ \tag{2.40}$$

Equation 2.40 can be used to propagate the F matrix through one period.

2.5 *Extended Eigenvectors*

There are cases where F is singular, and therefore has no inverse. In fact, that is the case with the halo orbit we have chosen to use. The Φ matrix has a repeated Poincaré exponent of zero (repeated eigenvalue of unity), with a ***dependent*** eigenvector. Since $F = [\vec{f}_1, \vec{f}_2, ...]$, any eigenvector, $\vec{f}_i$, which is not linearly independent of the others causes F to be rank deficient (singular). In our case, the F matrix had rank 5 instead of 6.

The generalised eigenvector presented a solution to our problem. For the setup of the generalized eigenvector problem, let us return to the predecessor of Eq. 2.37, which has no F^{-1} term (no requirement on F to be invertible).

$$\Phi(t, t_0)F(t_0) - F(t)e^{J(t-t_0)} = 0 \tag{2.41}$$

Note that the $e^{J(t-t_0)}$ takes the place of $\lambda_i I$ from Eq. 2.36. Let us use the Jordan form of the 2×2 block from the J matrix which contains the repeated zero value as an example (the Jordan form dictates the 1 on the superdiagonal):

$$e^{J\tau} = \exp\left\{\begin{array}{cc} 0 & 1 \\ 0 & 0 \end{array}\right\} = \left\{\begin{array}{cc} 1 & \tau \\ 0 & 1 \end{array}\right\} \tag{2.42}$$

where we have let $t = \tau$ and $t_0 = 0$. We now write it in column form and drop the time indices for convenience.

$$\Phi\{\vec{f}_1|\vec{f}_2\} - \{\vec{f}_1|\vec{f}_2\}\left\{\begin{array}{cc} 1 & \tau \\ 0 & 1 \end{array}\right\} = 0 \tag{2.43}$$

Now we multiply the terms above by columns, which leads to

$$\{\Phi\vec{f}_1|\Phi\vec{f}_2\} - \{\vec{f}_1|(\tau\vec{f}_1 + \vec{f}_2)\} = 0 \tag{2.44}$$

Since these two matrices are equivalent, their columns are equivalent and we can write

$$\{\Phi - I\}\vec{f}_1 = 0 \tag{2.45}$$

and

$$\{\Phi - I\}\vec{f}_2 = \tau\vec{f}_1 \tag{2.46}$$

Equation 2.45 is just a restatement of Eq. 2.36 where the Poincaré exponents are zero ($\omega_i = 0$) so $e^{\omega_i \tau} = 1$. In order to generalise Eq. 2.46 we write it as

$$(\Phi - \lambda_i I)\vec{f}_{i_{ext}} = \tau\vec{f}_{i_{rep}} \tag{2.47}$$

where $\vec{f}_{i_{rep}}$ is the repeated eigenvector and $\vec{f}_{i_{ext}}$ is the new, generalized, *extended* eigenvector. Note that the extended eigenvector, in order to satisfy Eq. 2.47, can be scaled by

$$\vec{f}'_{ext} = \vec{f}_{ext} + \alpha\vec{f}_{rep} \tag{2.48}$$

and it is therefore as non-unique as a normal eigenvector (which can be scaled by $\vec{f}'_{new} = \alpha\vec{f}_{old}$ — see (10)). We will now use Eqs. 2.36 and 2.47 in continuing our example to calculate the eigenvectors for the Φ matrix. First, the normal eigenvalue equation (Eq. 2.36) is used, giving us

$$\vec{f}_1 = \vec{f}_2 = span\begin{pmatrix} 1 \\ 0 \end{pmatrix} \tag{2.49}$$

The vector is repeated as expected. A generalized eigenvector is constructed using Eq. 2.47 giving us

$$\vec{f}_{ext} = span\begin{pmatrix} a \\ \tau \end{pmatrix} \tag{2.50}$$

where a is arbitrary and can be chosen to be zero (a must be zero if the new vector is to be perpendicular to the old one).

2.6 *Results of the Eigenvalue-Eigenvector Problem*

The eigenvalues of the monodromy matrix, $\Phi(\tau, 0)$, for the halo orbit were found and converted into Poincaré exponents. The Poincaré exponents are as follows

$$\omega_i = \left\{ \begin{array}{l} -2.4373955014588 \\ 2.4373955019038 \\ -.026092033595943i \\ .026092033595943i \\ 0.0 \\ 0.0 \end{array} \right\} \tag{2.51}$$

The first two exponents are real, the next two imaginary and the last ones will be referred to as the zero modes. The software which produced these exponents (the eigenvalue-eigenvector package in the IMSL library called "devcrg") did not give them to us in this order, so we regrouped them for ease of discussion. The order is quite arbitrary as long as each exponent is associated with the proper eigenvector. It should also be noted that the software did not give exactly zero for the zero exponents. As Wiesel and Pohlen stated (10: 4), "It is up the worker in this area to recognize this case, and substitute the correct values."

The Poincaré exponents are constant characteristics of the orbit in the three-body problem. The negative real exponent represents the stable mode. The positive real is unstable. Both of the imaginary exponents represent oscillatory modes. The zero exponents represent only a different epoch of the same orbit, and are neither stable nor unstable. Within the linear region, plots of the first two modes against each other look like a saddle point. Plots of the second pair are circles and the last two remain constant in time. This analysis of the modes is the basis of the modal control schemes presented in Chapters IV and V.

Associated with each of the exponents is an eigenvector, the combination of which is the modal matrix, $F(t)$, which was used in the similarity transformation

described in section 3.1. The matrix itself is very cumbersome and it is periodic (for the periodic orbit), which means that it is different at every time, t, but at the initial time it is given by

$$F(0) = \left\{ \begin{array}{ll} -2.374442084986946E-01 & -2.374442084873532E-01 \\ 2.041548870256156E-01 & -2.041548869917724E-01 \\ 8.904551229102137E-03 & 8.904551230670204E-03 \\ -9.274729220416125E-01 & 9.274729220687803E-01 \\ 1.938588253107533E-01 & 1.938588252272955E-01 \\ 6.383160385046611E-02 & -6.383160385939196E-02 \end{array} \right.$$

$$\begin{array}{ll} -1.340603252397338E-02 & -1.407327854914285E-27 \\ 4.197004838119940E-09 & 6.549857854528899E-01 \\ 4.606002014311875E-01 & -2.845632307073551E-09 \\ -3.420895405951368E-09 & -5.406149540610001E-01 \\ 2.049158967689975E-01 & -7.710108270570280E-10 \\ -5.203976092078526E-10 & -1.562251589378517E-01 \end{array}$$

$$\left. \begin{array}{ll} 0.000000000000000E+00 & -2.217844788884213E+01 \\ 7.415056092412337E-01 & 2.871181813841697E-08 \\ 0.000000000000000E+00 & -1.495894728274239E+02 \\ -5.936711168454215E-01 & -2.530885149026978E-08 \\ 0.000000000000000E+00 & 5.398535426318291E+01 \\ 3.126084395650520E-01 & -1.161680356454845E-07 \end{array} \right)$$

The last column is the extended eigenvector.

2.7 Summary

We have equations of motion and of variation for a particle in a three-body orbit. Using ISEE-3 data, we have found a periodic orbit to put our satellite into.

We have evaluated the Poincaré exponents, and using extended eigenvectors we have found an initial eigenvector matrix, $F(0)$, which has full rank.

III. Theory

3.1 Canonical Transformations

In order to do perturbation work on Hamiltonian systems, it is often quite desirable to transform the system into another set of variables which simplify the construction. If the transformation preserves the Hamiltonian structure of the system, it is called a canonical transformation. It is sometimes possible, in fact, to transform to a set of variables in which the Hamiltonian of the system vanishes identically. Such a transformation solves the problem, and the variables are ideal for use in perturbation work since the solved part of the problem no longer encumbers the statement of the dynamics. We were not so ambitious as to try and solve the problem because the RTBP cannot be solved in closed form — see Szebehely (7: 7). Our goal was to transform the problem into a set of variables that allowed the fundamental modes to be independent of one another. If Φ were diagonal, the subspaces, or modes, of Φ would be independent, and that is what led us to the eigenvalue-eigenvector problem in Chapter 2. This set of variables is called *modal* variables, and will be designated η_i. Wiesel and Pohlen (10) showed how to do canonical transformations in Hamiltonian systems for the non-degenerate case and several degenerate cases which appear in the RTBP. The transformation to modal variables is done by noting that F is the modal matrix, which transforms the Φ matrix to diagonal form according to

$$\Lambda = F^{-1}\Phi F. \tag{3.1}$$

This is nearly a restatement of Eq. 2.41 where e^{Jr}, the exponential of the Jordan form, takes the place of Λ, the diagonal matrix. We define

$$\delta x(t) = X(t) - X_p(t) \tag{3.2}$$

to be a small variation in the state vector at a particular time. $X_p(t)$ is the state vector for the periodic orbit, and $X(t)$ is the state vector for a nearby orbit, not necessarily periodic. A nearby orbit is one whose state vector is close to that of the periodic orbit. Note that $\delta x(t)$ is a vector of length six called the *variation* of X. Then

$$\delta x(t) = F(t)\eta(t) \tag{3.3}$$

where $F(t)$ is the modal matrix at that particular time so the transformation is simply a matter of solving for $\eta(t)$

$$\eta(t) = F^{-1}(t)\delta x(t) \tag{3.4}$$

The modal variables approach zero as the state vector approaches the periodic orbit. The value of each mode changes with time, giving a plot of the modes a characteristic shape, and a characteristic e-folding time, according to its Poincaré exponent. The e-folding time is the amount of time required for the mode to change by a factor of e. Plots of the mode shapes will be shown in the next chater.

3.2 Fourier Representations

In order to control the satellite with modal control, it was necessary to evaluate the modal variables at arbitrary times during the simulation. Since $F(t)$ varies with time (it is periodic), but not according to a simple function, there had to be a way to obtain values in double precision for the 6×6 matrix at arbitrary times. This was accomplished by using a truncated Fourier series. Each member of the periodic matrix F was stored as a table of sine and cosine coefficients so that any given value of the matrix, f_{ii}, was given by

$$f_{ii} = \sum_{j=0}^{N} c_j \cos(j\omega t) + \sum_{k=1}^{N} s_k \sin(k\omega t). \tag{3.5}$$

This sum could be evaluated at any time during the simulation, which allowed access to any $F(t)$ without re-integrating Eq. 2.40. The values for the periodic orbit were stored and retrieved in the same way after they were obtained by integrating the equations of motion and variation in the beginning of the project. For all the calculations done in this study, 25 coefficients were used and each coefficient was calculated and stored to 13 decimal places. This provided all the accuracy needed for the calculations, but there were instances where the truncation of the Fourier series representations became apparent. Chapter IV shows some graphs (see figure 4.6) that may indicate anomalies due to this approximation.

IV. Controllers

4.1 The Halo Orbit

The halo orbit is inherently unstable. Using initial conditions which were correct to within ten centimeters in position and a like amount in momentum, the satellite left the nominal orbit completely before it had completed its fourth revolution (see Figure 4.1). When evaluating the relative stability of the orbit like this, care must be taken that enough integration steps are used. If the steps are not sufficiently close together, the errors in the integration can appear to be inherent instabilities in the orbit. The integration package used was a fourth order predictor-corrector (9). It required about 2000 integration steps per orbit to assure that the errors were smaller than the instability so the true instability was revealed. The divergence shown here resulted from a tiny error in the initial conditions, which grew (exponentially in the unstable modal direction) until the satellite literally coasted off into space.

4.2 The "Cheater" Controller

The "Cheater" Controller was devised as a way to stabilize the orbit through several periods so that the long term behavior of the orbit and its modes could be analyzed and visualized. The controller worked by resetting to zero the unstable mode any time that it reached a threshold value. This was accomplished by subracting from the state vector the fraction of the corresponding unstable eigenvector equal to the magnitude of the threshold.

$$X(t_i)_{new} = X(t_i)_{old} - \varepsilon \vec{f}(t_i)_{unstable} \tag{4.1}$$

where ε is the threshold value. This simple concept, while not a realistic controller, validated the concept of modal analysis by demonstrating that the modes were independent of one another since a change in the state vector in the direction of the

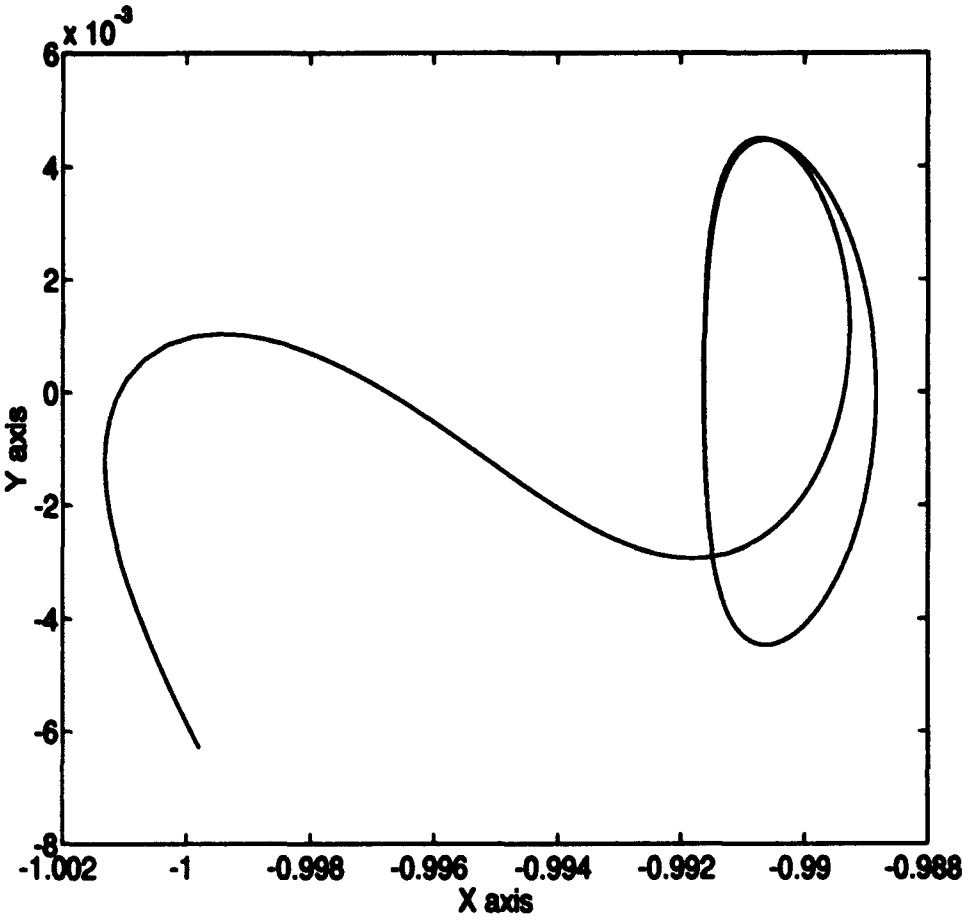

Figure 4.1. X — Y Projection of Orbit Showing that the Satellite does not Remain Close to the Nominal Orbit. The Earth is at About X = -1, Y = 0.

unstable mode did not affect the other modes. Using this controller we were able to propagate the orbit for as long as desired, since it was not allowed to diverge. This was important because it turned out that the oscillatory mode had a period of about seventy times the orbital period. Figure 4.2 shows the two imaginary (oscillatory) modes plotted against each other for about 99 orbital periods (99τ). During a simulation of only a few times τ, the oscillation completes only a portion of the circle seen in the figure. The initial conditions for this simulation were perturbed in the direction of one of the oscillatory modes by a factor of 10^{-7} so that the mode did not just hover about zero. The orbit was controlled using the "cheater" controller with the threshold set to 10^{-7}.

The reason this controller is unrealistic is that the entire state vector was repositioned during the "maneuver". In reality, it is only possible to change the momentum states using thrust. The concept of changing a position state instantaneously corresponds to teleportation. While perhaps desirable, it is not possible, so we were then forced to look at a more feasible alternative.

4.3 Maneuver Optimization

A realistic controller is an order of magnitude more complex. The cheater had the advantage of moving the state vector in the direction of an eigenvector, affecting only one mode. Whatever we do with an actual maneuver will affect the state vector in a somewhat more unpredictable way than our cheater did. If we are to obtain the desired response in one mode, we will have to sacrifice some response in the others. This amounts to the statement of an optimization problem, and indeed, in this chapter we attempted to optimize control by two separate strategies. The first is described in this section, and the second in the next.

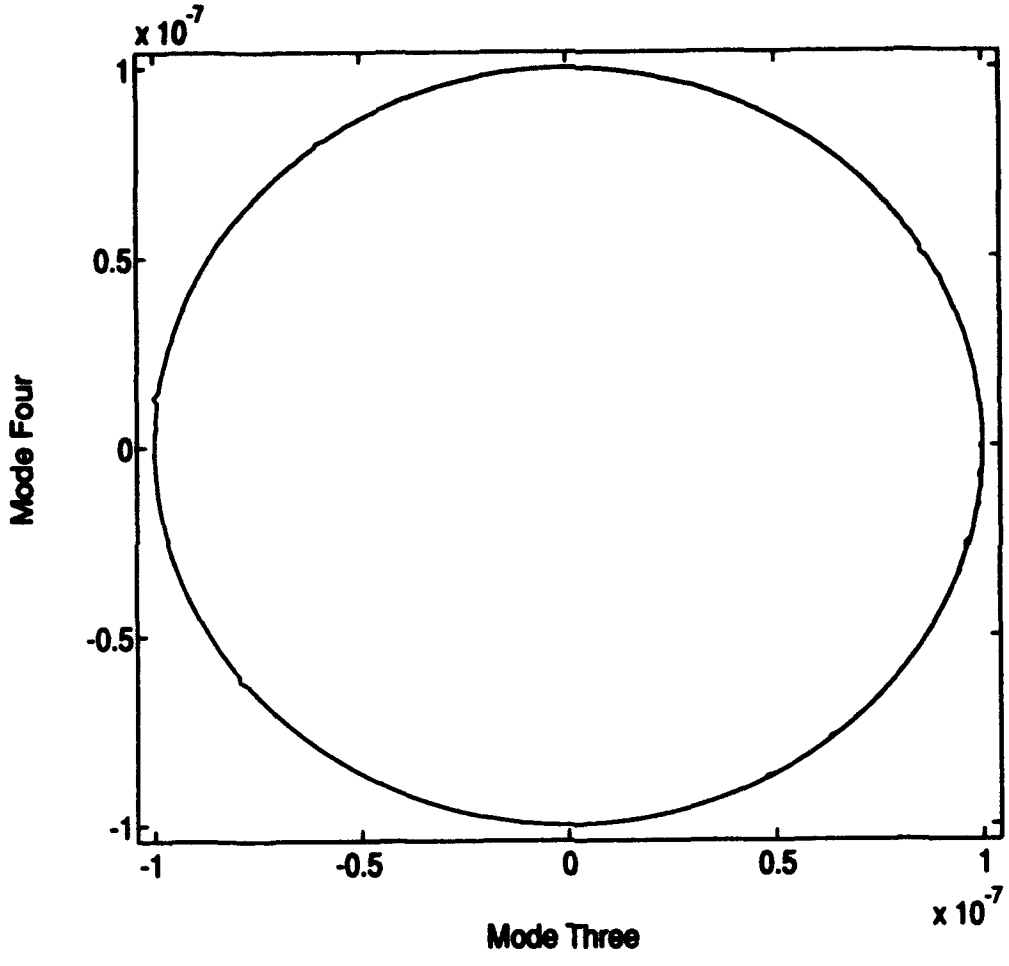

Figure 4.2. Oscillatory Modes Plotted Against One Another for 99 Periods

Let the vector of permissible maneuvers be expressed as a particular variation of the state vector, $\delta X_{permissible}$. Then

$$\delta X_{permissible} = \{0 \;\; 0 \;\; 0 \;\; \delta p_x \; \delta p_y \; \delta p_z\}^T \tag{4.2}$$

since only the momentum states can be affected by an impulsive maneuver. Recall the transformation to modal variables from Eq. 3.4.

$$\eta = F^{-1}\delta X \tag{4.3}$$

We can then write the change in modal variables as

$$\delta\eta = F^{-1}\delta X \tag{4.4}$$

where the δ notation is used here to denote a maneuver (a change in state). When we write each of the components, it looks like this

$$\begin{pmatrix} \delta\eta_1 \\ \delta\eta_2 \\ \delta\eta_3 \\ \delta\eta_4 \\ \delta\eta_5 \\ \delta\eta_6 \end{pmatrix} = \begin{Bmatrix} F^{-1}_{1,1} & F^{-1}_{1,2} & F^{-1}_{1,3} & F^{-1}_{1,4} & F^{-1}_{1,5} & F^{-1}_{1,6} \\ F^{-1}_{2,1} & \cdots & & & & \\ \vdots & \ddots & & & & \\ \vdots & & & & & \\ \vdots & & & & & \\ \vdots & & & & & \end{Bmatrix} \begin{pmatrix} 0 \\ 0 \\ 0 \\ \delta p_x \\ \delta p_y \\ \delta p_z \end{pmatrix} \tag{4.5}$$

Where $F^{-1}_{i,j}$ are the components of F^{-1} (and not the inverse of the components of F). Note that we will be required to compute the actual inverse of the modal transformation matrix, F, for the first time. Before, we had always been able to solve the linear algebra problem for the modal variables by Gaussian elimination and back substitution without computing the inverse (see Chapter III). Since $\delta\eta_1$ is the variation in the unstable mode, we are interested in the elements of F^{-1} which

both contribute to the value of $\delta\eta_1$ and multiply the permissible elements of δX. These are $F^{-1}_{1,4}$, $F^{-1}_{1,5}$ and $F^{-1}_{1,6}$. This constitutes a single scalar equation

$$\delta\eta_1 = F^{-1}_{1,4}\delta p_x + F^{-1}_{1,5}\delta p_y + F^{-1}_{1,6}\delta p_z \tag{4.6}$$

Just as in the "cheater" controller, we would like to annihilate the unstable mode. Mathematically,

$$\delta\eta_{1,desired} = -\eta_1. \tag{4.7}$$

The desired change (maneuver) in the first modal variable is to negate its present value. This constitutes a second scalar equation. We are now ready to formally state the optimisation problem. We wish to minimise the fuel used for station-keeping. We will use ΔV per unit time as the figure of merit to evaluate the controllers. The controller will minimise $P = (\Delta V)^2$ for each maneuver. Stated mathematically, we will minimise Eq. 4.8 subject to Eq. 4.9.

$$P = \delta p_x^2 + \delta p_y^2 + \delta p_z^2 \tag{4.8}$$

$$\delta\eta_1 + \eta_1 = 0 \tag{4.9}$$

Substituting from Eq. 4.6 for the value of $\delta\eta_1$ and introducing a Lagrange multiplier, λ, allows us to write the problem in one equation.

$$P = \delta p_x^2 + \delta p_y^2 + \delta p_z^2 + \lambda(F^{-1}_{1,4}\delta p_x + F^{-1}_{1,5}\delta p_y + F^{-1}_{1,6}\delta p_z + \eta_1) \tag{4.10}$$

Taking partial derivatives of P with respect to the permissable changes in the state and setting them equal to zero yields

$$\begin{aligned}
\frac{\partial P}{\partial(\delta p_x)} &= 0 = 2\delta p_x + \lambda F_{1,4}^{-1} \quad \Rightarrow \quad \delta p_x = -\tfrac{1}{2}\lambda F_{1,4}^{-1} \\
\frac{\partial P}{\partial(\delta p_y)} &= 0 = 2\delta p_y + \lambda F_{1,5}^{-1} \quad \Rightarrow \quad \delta p_y = -\tfrac{1}{2}\lambda F_{1,5}^{-1} \\
\frac{\partial P}{\partial(\delta p_z)} &= 0 = 2\delta p_z + \lambda F_{1,6}^{-1} \quad \Rightarrow \quad \delta p_z = -\tfrac{1}{2}\lambda F_{1,6}^{-1}
\end{aligned} \tag{4.11}$$

and with respect to the Lagrange multiplier

$$\frac{\partial P}{\partial \lambda} = 0 = \delta\eta_1 + \eta_1 \Rightarrow \delta\eta_1 = -\eta_1. \tag{4.12}$$

Note that Eq. 4.12 is simply a restatement of the constraint. From the right hand side of Eq. 4.11 we know the direction of our maneuver since we know the proportion in each of the momentum directions, but its magnitude is scaled by λ, which we do not know. In order to solve for it, let us rewrite Eq. 4.11.

$$\delta\vec{p} = \begin{pmatrix} \delta p_x \\ \delta p_y \\ \delta p_z \end{pmatrix} = -\frac{1}{2}\lambda \begin{pmatrix} F_{1,4}^{-1} \\ F_{1,5}^{-1} \\ F_{1,6}^{-1} \end{pmatrix} \tag{4.13}$$

Then note that Eq. 4.6 can be rewritten as

$$\delta\eta_1 = (F_{1,4}^{-1} \;\; F_{1,5}^{-1} \;\; F_{1,6}^{-1})\delta\vec{p} \tag{4.14}$$

Substituting from Eq. 4.13 for the value of $\delta\vec{p}$ we have

$$\delta\eta_1 = -\frac{1}{2}\lambda[(F_{1,4}^{-1})^2 + (F_{1,5}^{-1})^2 + (F_{1,6}^{-1})^2] \tag{4.15}$$

We know from the constraint that $\delta\eta_1 = \eta_1$, so solving for λ

$$\lambda = \left[\frac{2\eta_1}{(F_{1,4}^{-1})^2 + (F_{1,5}^{-1})^2 + (F_{1,6}^{-1})^2}\right] \tag{4.16}$$

The control scheme, then, consisted of evaluating the unstable mode until a threshold was reached. Since the unstable mode grows exponentially with time, we knew it would not decrease. A realistic impulsive maneuver was planned according to the mathematics presented in this section which optimised the direction and the magnitude of the maneuver to zero out the unstable mode. The equations of motion were then propogated from that point, with initial conditions given by the conditions at maneuver, plus the maneuver (the change in momentum states), until the unstable mode again reached the threshold.

4.4 Results of the Realistic Controller

The results using this controller are displayed in graphical form in the following figures. We begin with a medium threshold, allowing the unstable mode to reach a value of 10^{-7}. See Figure 4.3. This threshold was chosen because its results are a good compromise between low cost and frequency of maneuvers. A lower cost can be obtained, but it requires more frequent maneuvering. The average normalised cost of the maneuvers approaches a level value after about 40 time units which is a little over 13 orbits and about six and a half years. The simulations in this section were run for a total of 100 time units–some 30 orbits over about 15 years. The average cost for maintaining the orbit for this first threshold is about 0.6 cm/sec per year. Each of the maneuvers is about 0.4 cm/sec in magnitude and they occur with a frequency of just less than once per orbit (just under twice a year).

Figure 4.4 shows the performance of the same controller with a lower threshold of 10^{-9}. Here, the maneuvers are happening with greater frequency (about double–average is 1.7 maneuvers per orbit, which is 3.4 maneuvers per year), but

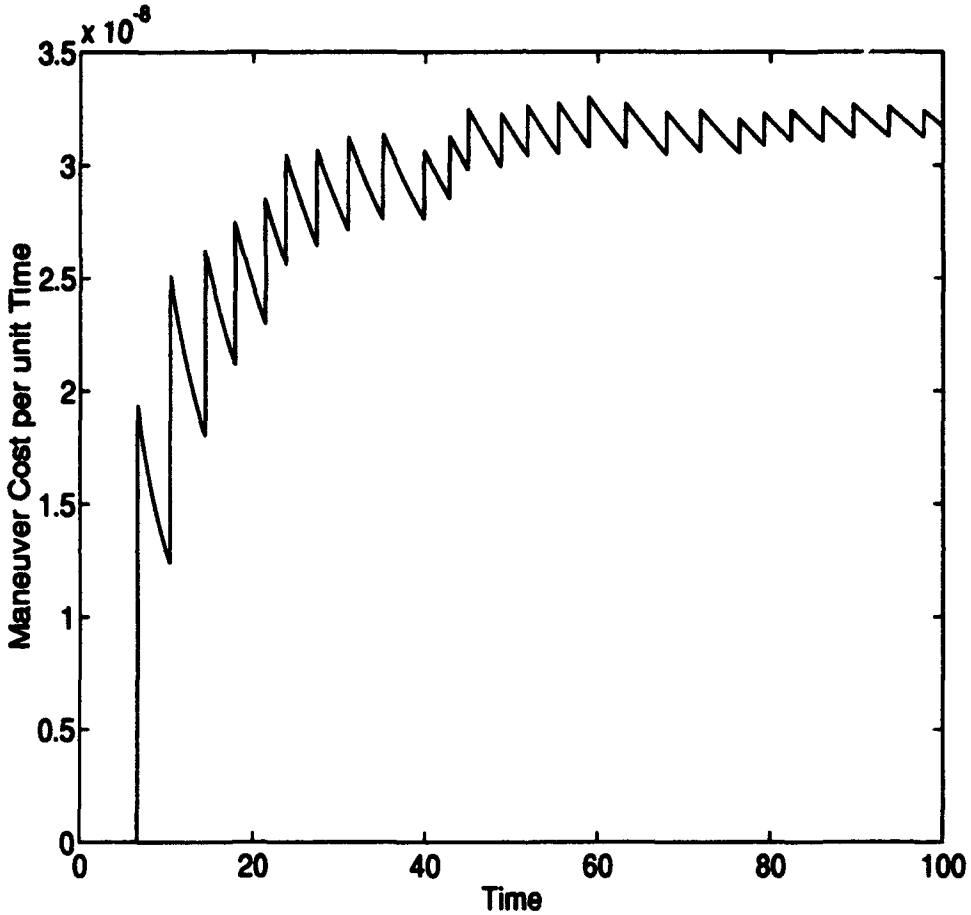

Figure 4.3. Average Maneuver Cost as a Function of Time (Canonical Units), Threshold = 10^{-7}

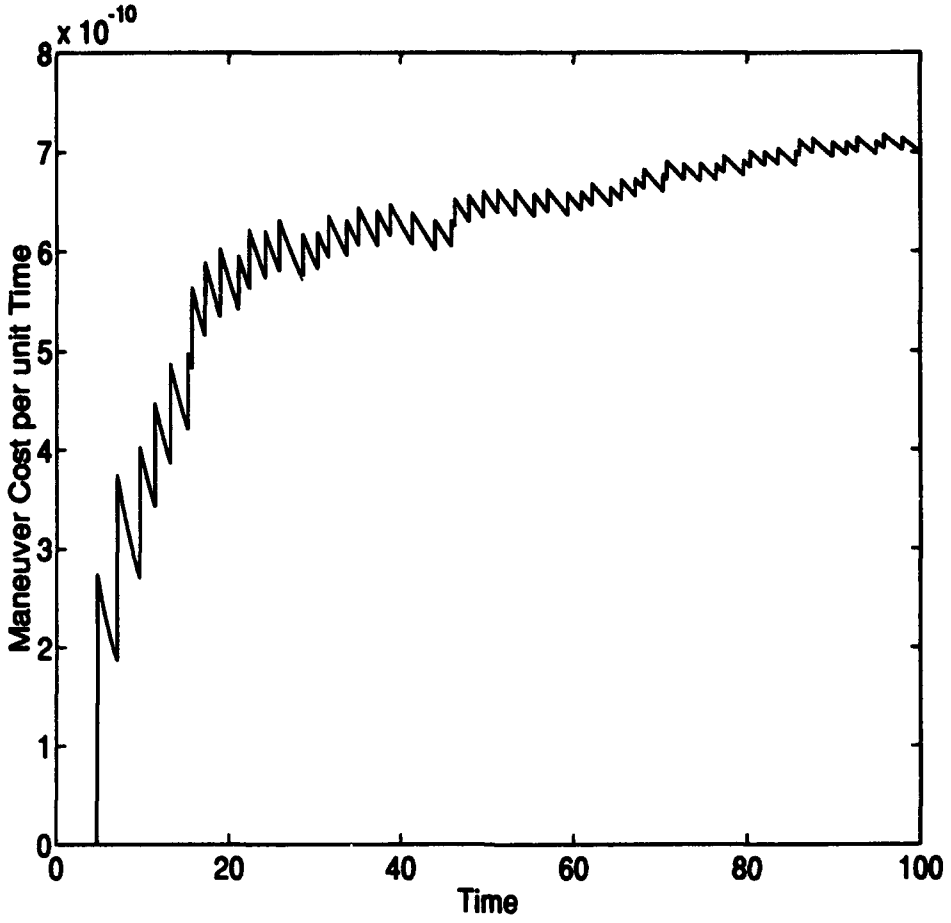

Figure 4.4. Average Maneuver Cost as a Function of Time (Canonical Units), Threshold = 10^{-9}

the magnitude of each maneuver is much smaller (they average about 0.0037 cm/sec). The total average cost is only 0.013 cm/sec per year–about 1/50th what it was to maintain it with the higher threshold. Now let us look at the behavior of the modes during this control process. Figure 4.5 is a plot of the two real modes, corresponding to the positive real Poincaré exponent (unstable mode) and the negative real exponent (stable mode). The general shape of the plot may be a bit deceiving at first. The diagonal lines are drawn where the maneuver occurs. The unstable mode is brought back to (approximately) zero, but the stable mode acquires an unknown

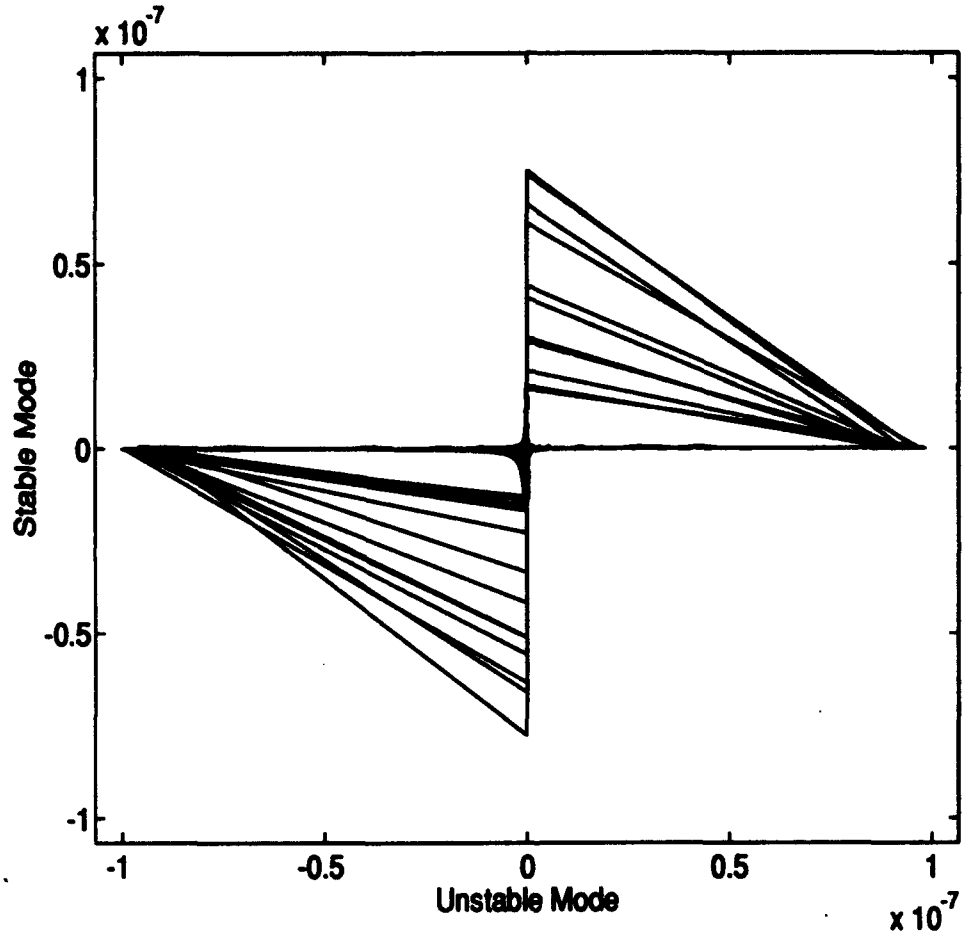

Figure 4.5. Plot of the Two Real Modes as the Realistic Controller Operates, Threshold = 10^{-7}

positive or negative value (remember we can only change momentum states, so the controller affects other modes). As the orbit progresses, the stable mode approaches zero while the unstable mode diverges. This creates a saddle shape in the center of the plot, as shown by Figure 4.6. The spikes in the figure are due to numerical errors in calculating the modes (possibly truncation error in the Fourier coefficients). Larger values of the modes are less affected by these errors, while smaller values are nearly obscured by them. Figure 4.7 would look very messy if all the dots were connected because of the large errors near the origin, but as a series of dots, it still shows the same progression in the real modes. The unstable mode is never allowed to exceed 10^{-9} in absolute value.

It would be interesting to see what would happen if we tried to reduce the number of maneuvers further by increasing the threshold. We could allow the unstable mode to get larger before imposing control. Figure 4.8 shows that the cost continues to increase as time progresses for a threshold of 10^{-3}. Although the first maneuver happens later than it does with a smaller threshold, they come more frequently after the first two or three. This is not hard to understand if you look at the plot of the real modes in Figure 4.9, which shows that the modes are really no longer in the linear region where they behave like a saddle point and where they can be controlled. The controller still does not allow the unstable mode to exceed the threshold, but this is insufficient to control the orbit in this nonlinear region. One interesting thing about this control scheme was that the orbit itself did not remain the same. Figure 4.10 shows the view of the orbit that we would get from the earth. It remained a halo orbit for about three and a half periods, and then began to change. It was under some control, however, because it failed to diverge completely. Its apparent direction reversed as the plane of the orbit revolved. The worst thing about this situation was that the satellite crosses the sun's disk, which was completely unacceptable. The sun would appear at the center of the plot, about 1 inch in diameter. The cost diverged

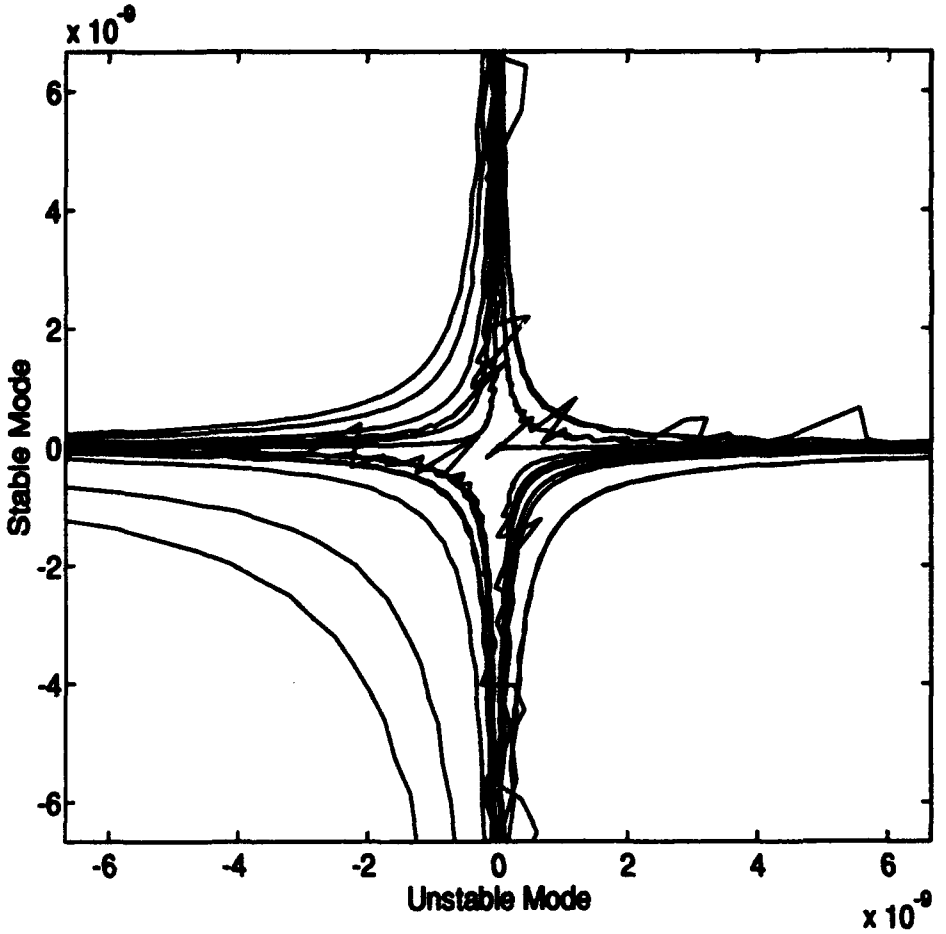

Figure 4.6. Close-Up of the Two Real Modes for 100 Time Units as the First Realistic Controller Operates Showing the Saddle Behavior, Threshold $= 10^{-7}$

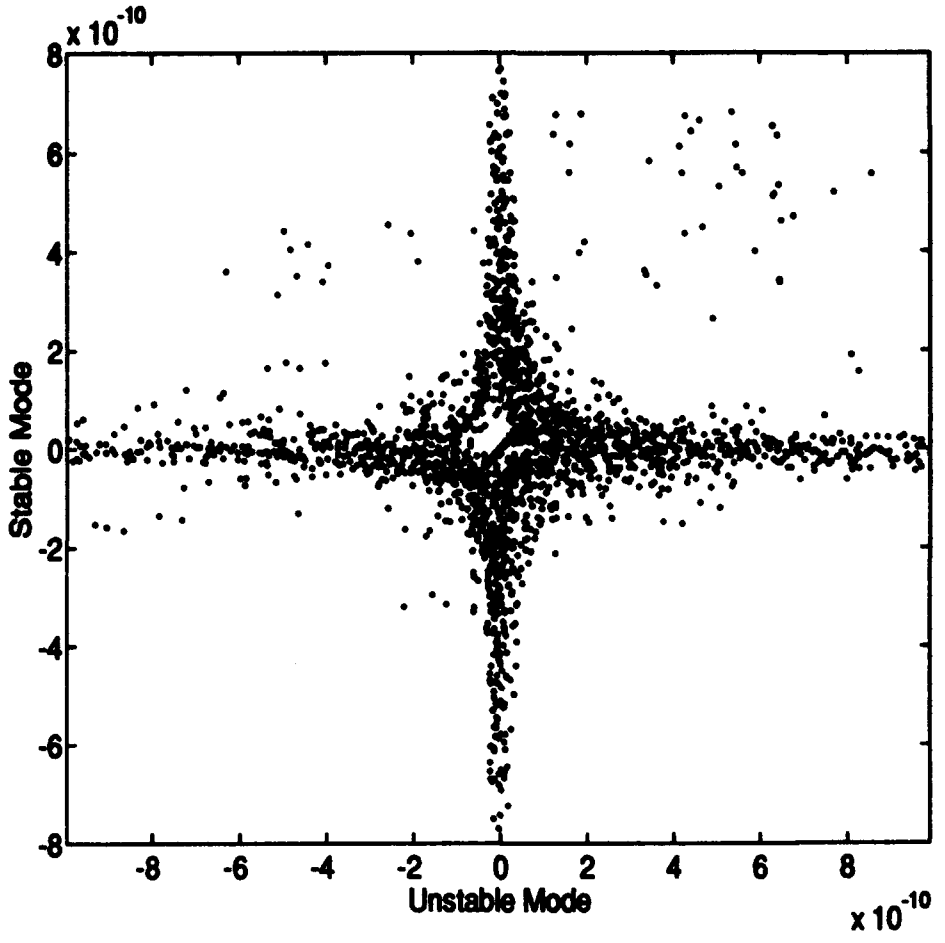

Figure 4.7. Plot of the Two Real Modes as the Realistic Controller Operates Showing the Saddle Behavior, Threshold = 10^{-9}

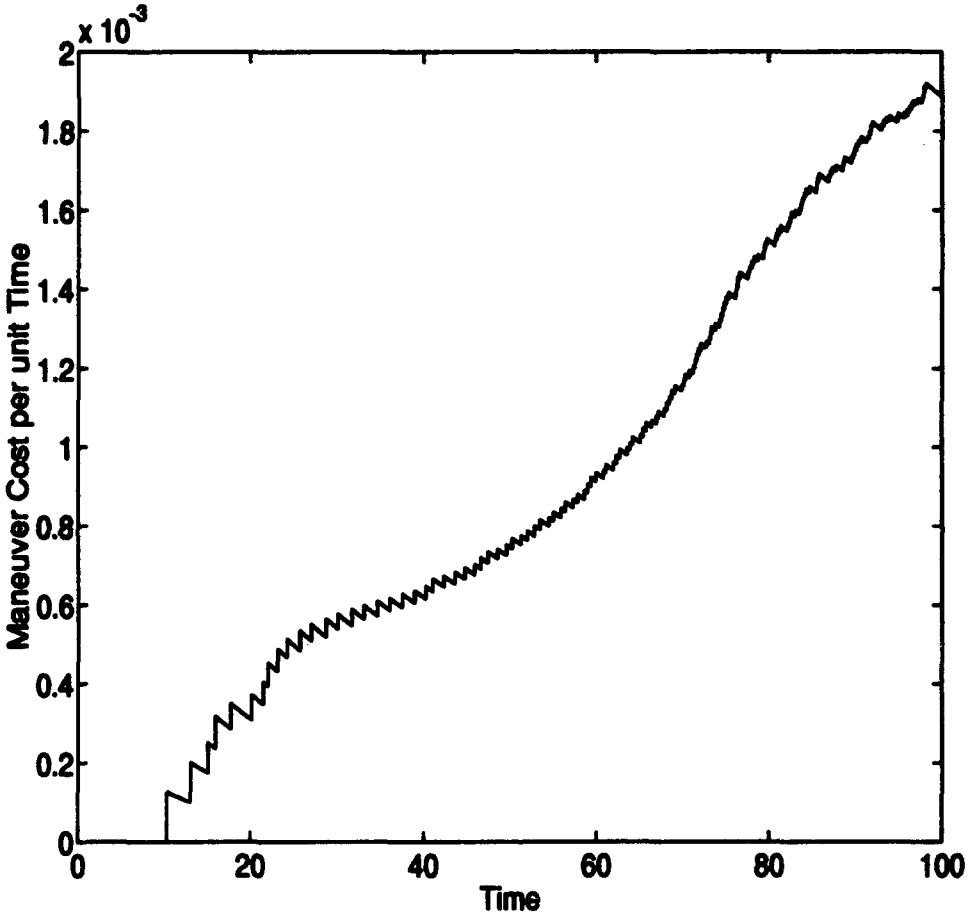

Figure 4.8. Average Maneuver Cost as a Function of Time, Threshold = 10^{-3}

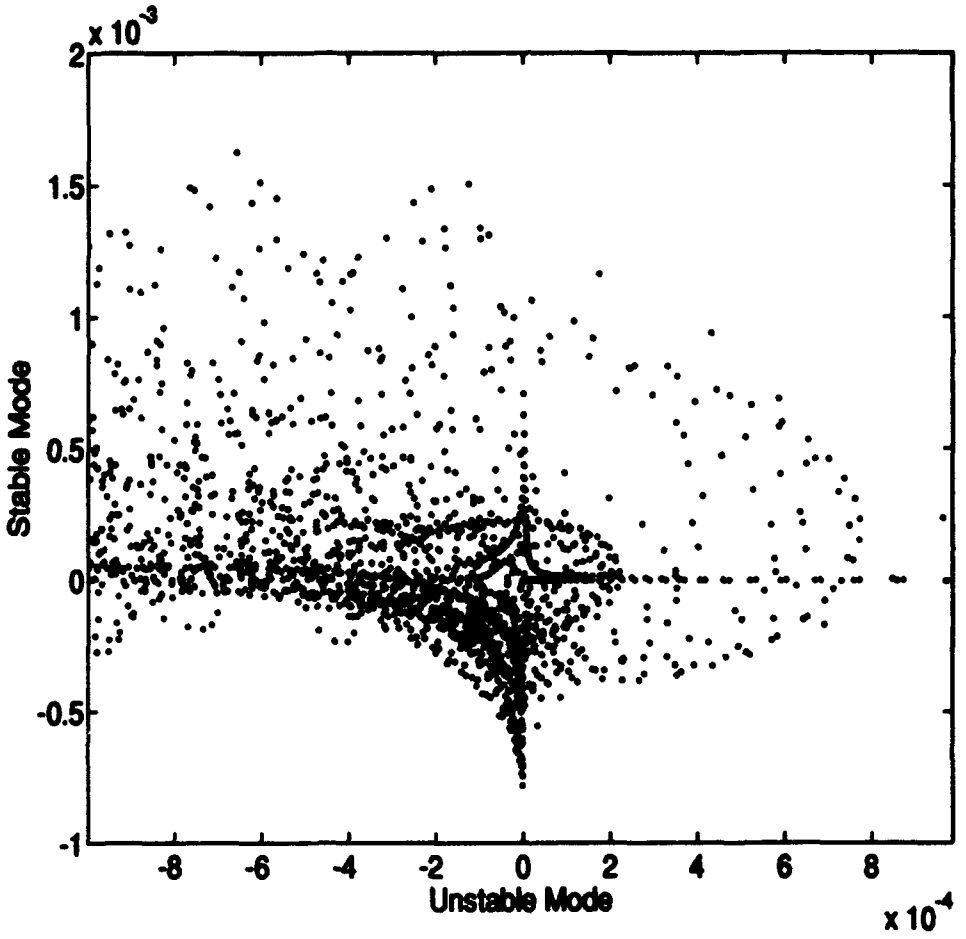

Figure 4.9. Plot of the Real Modes for an Insufficient Amount of Control, Threshold = 10^{-3}, Showing Nonlinear Behavior of the Modes

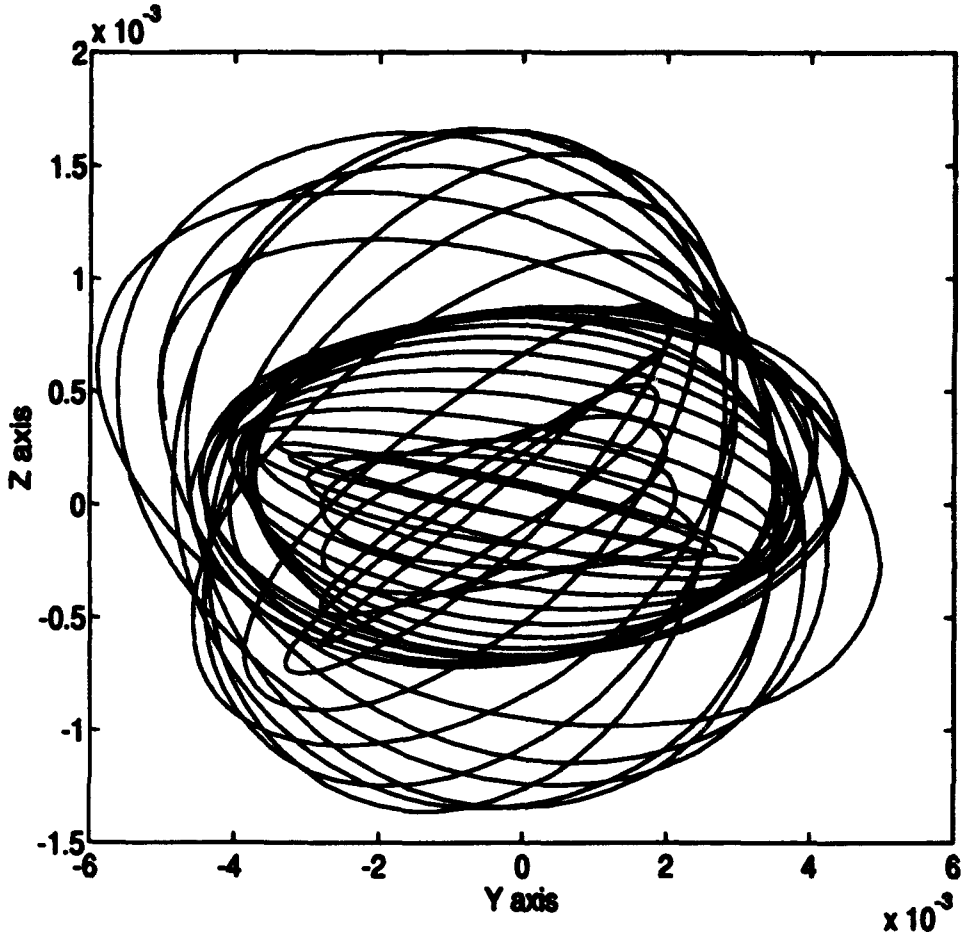

Figure 4.10. **Plot of the Y – Z Projection of the Orbit, Threshold = 10^{-3}, Showing that the Orbit Changes Radically While Remaining in Vicinity of L_2 (Origin)**

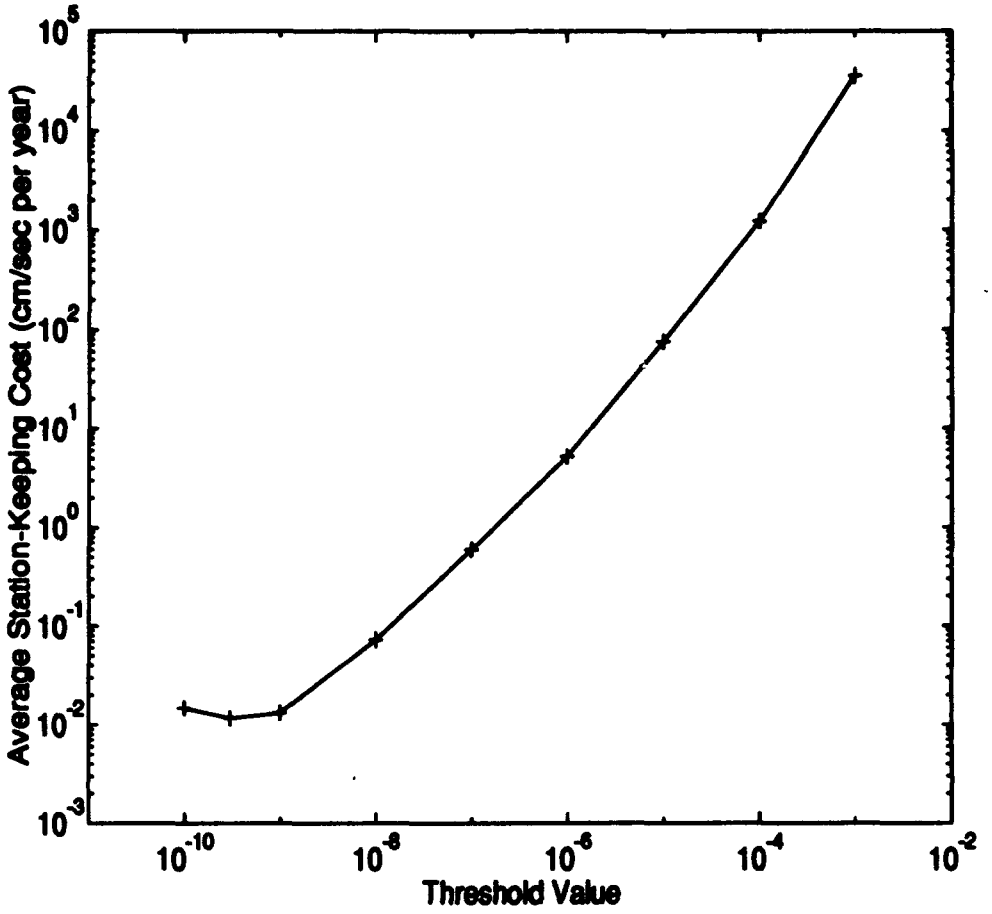

Figure 4.11. Performance of the Realistic Controller as a Function of the Controller's Threshold Value

and the satellite left its orbit. We concluded that the unstable mode could not be allowed to reach 10^{-3} in magnitude if we wished to control the satellite.

The figure of merit used to compare the control schemes is the average acceleration. Each maneuver is a velocity change, ΔV. The only way to objectively evaluate the performance of the controller is to normalize the total ΔV by the time elapsed, $\frac{\Delta V}{\Delta t}$, which is an average acceleration. Figure 4.11 shows the performance of this controller as a function of the threshold value. We can see that less maneuvering is required if the threshold is kept lower. The station-keeping cost has been

converted to units that are easy to understand (cm/sec per year) for this plot, but the horizontal axis is left in the original "modal" units, which are a transformation (by F^{-1}) of canonical units. Each point on the plot in Figure 4.11 represents a run (simulation) of the system, and is the final value of, for instance, Figures 4.3 and 4.4.

4.5 Optimization of Maneuver Epoch

In this section, a slightly different control scheme was attempted. Instead of immediately maneuvering whenever the unstable mode reached a threshold, the ideal time for a maneuver in the orbit was determined, and then a maneuver was executed at that time regardless of the instability. The optimal time for a maneuver is when the projection of the unstable mode onto the momentum direction is maximum so that a momentum change will produce maximum change in the unstable mode. The concept of optimizing the maneuver epoch *and* the maneuver direction and magnitude should give us a global optimum. It remains to be seen, however, whether that global optimum is suited to the problem. The reason it might not be is that the e-folding time of the unstable mode (time required for it to grow by a factor of e) is seven orders of magnitude shorter than the period of the orbit. This results in the growth of the unstable mode by a factor of e^7 (approximately = 1100) during one period.

The optimum time for a maneuver is when the maneuver itself would be smallest. In the development of the previous controller, we minimized the objective function, $P(=\Delta V^2)$, for whatever time in the orbit that the threshold happened to be exceeded. Now we wish to find a global minimum for ΔV regardless of the time or the value of the unstable mode. In order to find this global minimum, we remove the modal variable from the problem. The normalized value of λ becomes (see Eq. 4.16)

$$\lambda = \left[\frac{2}{(F^{-1}_{1,4})^2 + (F^{-1}_{1,5})^2 + (F^{-1}_{1,6})^2}\right] \tag{4.17}$$

and we know that the magnitude of the maneuver is given by

$$\Delta V = \sqrt{\delta p_x^2 + \delta p_y^2 + \delta p_z^2} \tag{4.18}$$

so substituting for the value of the $\delta p's$ from Eq. 4.11

$$\Delta V = \sqrt{(-\frac{1}{2}\lambda F_{1,4}^{-1})^2 + (-\frac{1}{2}\lambda F_{1,5}^{-1})^2 + (-\frac{1}{2}\lambda F_{1,6}^{-1})^2} \tag{4.19}$$

When we substitute from Eq. 4.17 for the value of λ, and perform the obvious cancellation, we see that

$$\Delta V = \sqrt{\lambda} \tag{4.20}$$

so that minimising ΔV is equivalent to minimising the normalised λ. It turns out that λ has a periodic nature, and has the same period as that of the orbit. Figure 4.12 shows the value of the normalised λ as a function of time for 10 time units (3.27 periods). Its value fluctuates between about 2.18 and 2.06, with a minimum occurring just once per orbit.

Knowing that λ was periodic and that it had a minimum during each orbit allowed us to use that fact in maneuvering the satellite. The control scheme evaluated λ at each point in the orbit, found where it had its minimum, and then executed a maneuver at that time. The maneuver was computed in exactly the same way as was done in section 4.3. The performance of the controller is shown graphically in Figure 4.13. Comparison of Figure 4.13 with Figure 4.3 shows that this method of maneuvering is actually a little less expensive (about 0.23 cm/sec per year) than the threshold controller with the threshold at 10^{-7}, but not as cheap as when the threshold is moved to 10^{-8}. Another advantage of the periodic controller here is that after the first maneuver (0.86 cm/sec), all the others were nearly identical in magnitude (the maneuver magnitude grew slowly from about 0.07 to 0.17 cm/sec) and direction, and they were all performed at the same point in the orbit. See

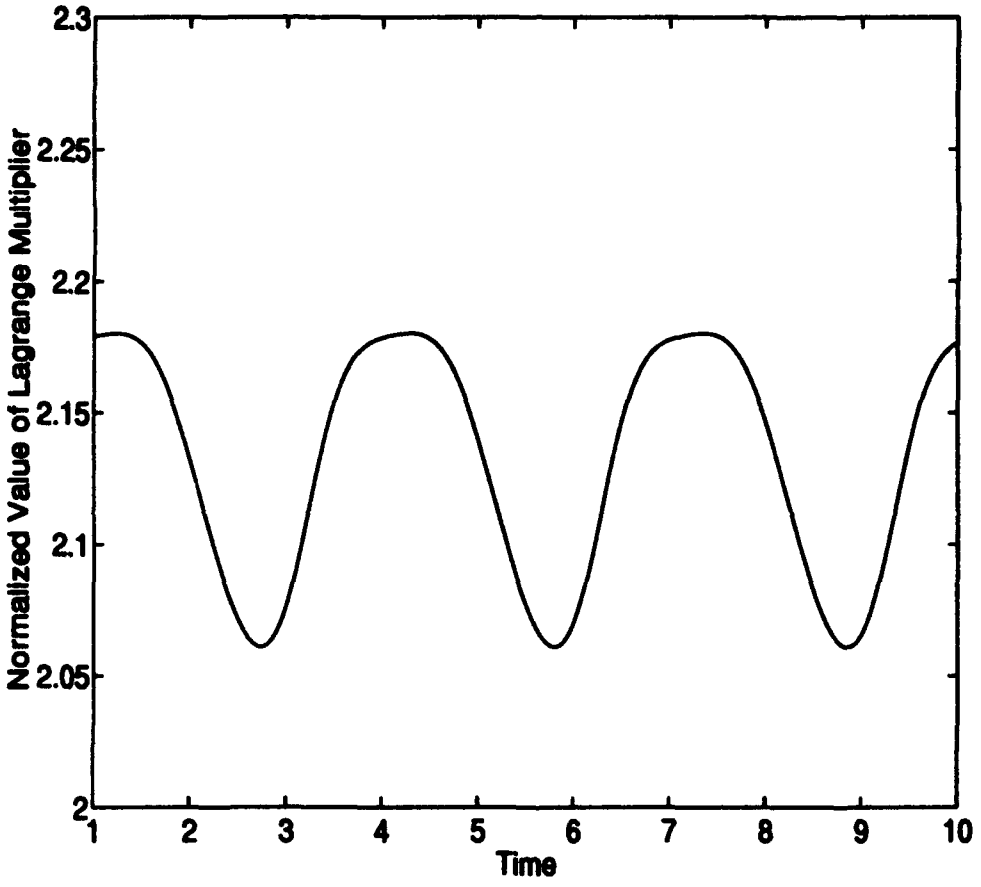

Figure 4.12. Plot of λ Versus Time for 3.3 Periods Showing its Periodic Nature with Minima Occurring Once per Orbit

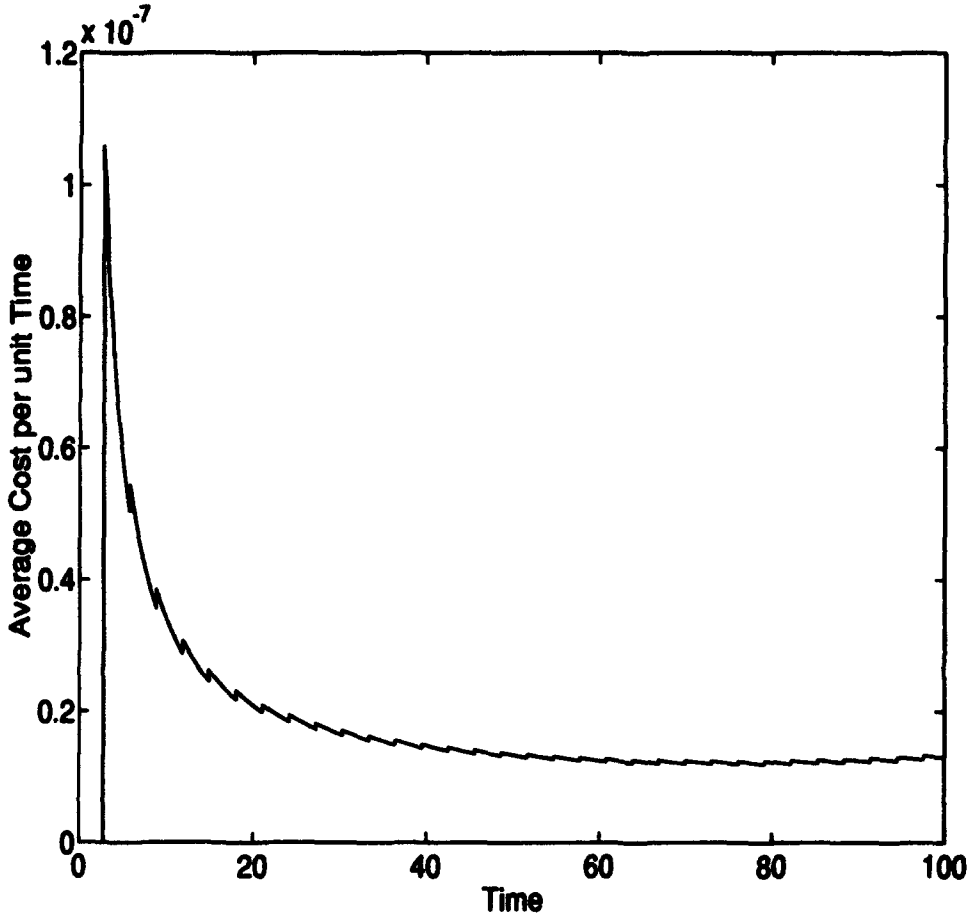

Figure 4.13. Average Maneuver Cost as a Function of Time While Maneuvering Once per Orbit at the Optimal Time

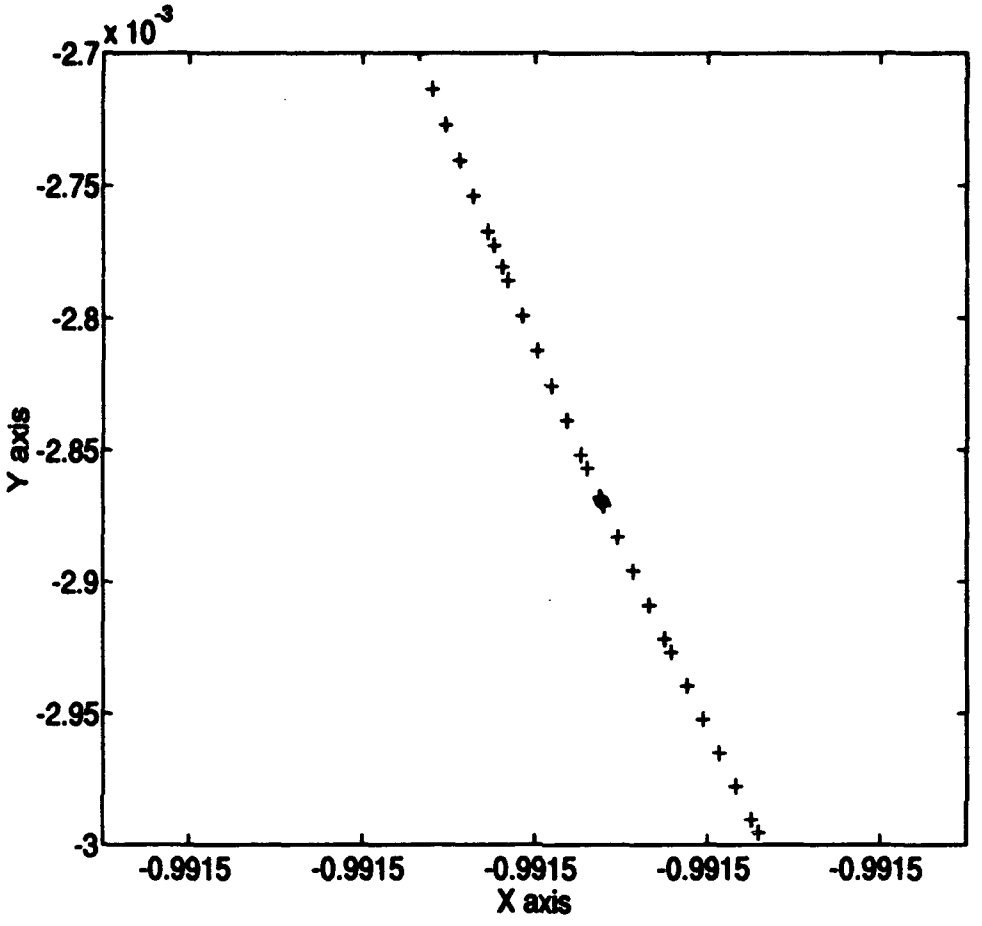

Figure 4.14. X – Y Projection Plot of the Maneuvering Portion of the Halo Orbit Under Periodic Control

Figure 4.14. The maneuvering point is where several points are plotted together in the middle of the trajectory shown. The velocity change at this point is so slight as to be invisible to the eye even at this scale, which shows about a hundredth of the orbit.

The performance of this controller was somewhat disappointing. While the concept of the optimum maneuver epoch was validated (it worked), it was not overall the cheapest way to control the satellite in its orbit. It was not therefore a global optimum for the control problem. A low threshold (say 10^{-8}) was cheaper by an

order of magnitude. If λ had had a greater range, so that there was a point in the orbit at which it was much cheaper to maneuver, then this optimum would have held greater promise for inexpensive maneuvering. As it is, the optimum epoch for maneuvers will not be pursued further.

4.6 Behavior of the Other Modes

While it is not strictly on the critical path to controlling the satellite, the behavior of the other modes under control is interesting to note and will therefore be included here briefly. It was noted in section 4.2 that the oscillatory modes would strictly oscillate about the origin if the unstable mode could be independently controlled within the linear region (see Figure 4.2). If, however, the unstable mode is controlled with some dependence on the other modes (as it was with the realistic controllers), we might wish to know what the the crossover effect will be.

Let us look at Figure 4.15. During each of the maneuvers there is a discontinuity in the plot, shown with a straight line (more or less horizontal lines). Between maneuvers, when the satellite is drifting freely, the imaginary modes tend to continue on their characteristic circles (nearly vertical arcs on the graph). The period of the imaginary mode oscillation is so long that only a short segment of the circle is completed before the next maneuver. The value of the imaginary modes appears somewhat random, but it increases slowly over the course of the simulation.

Figure 4.16 is the analog of the previous figure, with the zero modes plotted instead of the imaginary modes. When the satellite is drifting freely, the value of the modes remains relatively constant (these appear as vertices on the graph), and when a maneuver is performed, their value changes slightly (the whole plot is on the order of 10^{-8}) in the direction of the maneuver, to remain there until next maneuver.

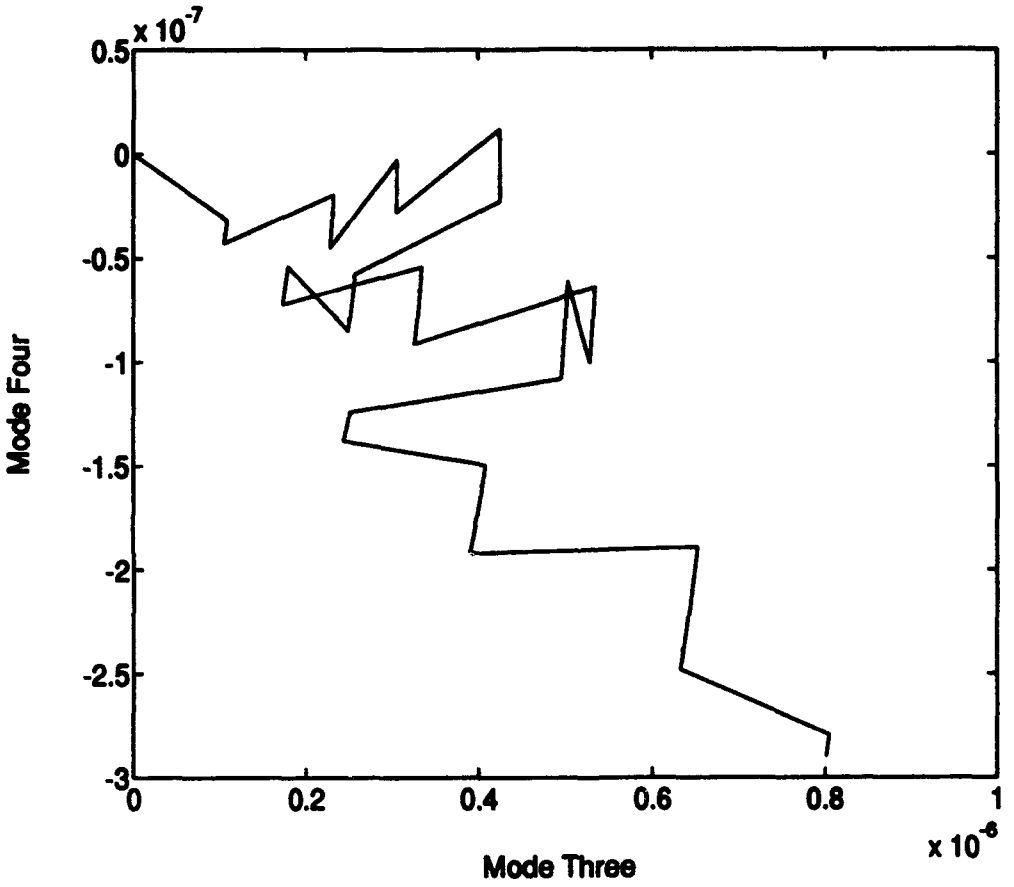

Figure 4.15. Imaginary Modes Plotted Together While Satellite is Under Realistic Control

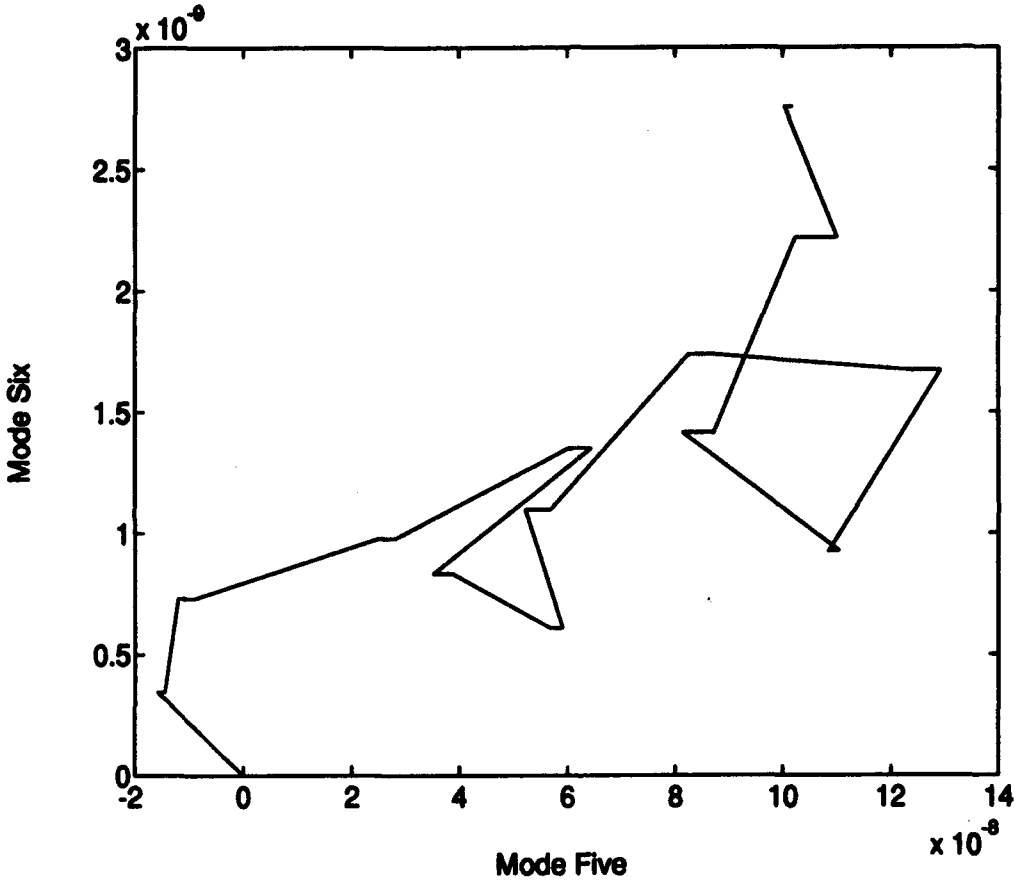

Figure 4.16. Zero Modes Plotted Together While Satellite is Under Realistic Control

4.7 Summary

It has been demonstrated that the satellite in the three-body halo orbit can successfully be controlled (kept near the periodic orbit) by observation and manipulation of its modal states with little attention being paid to its actual position in space or velocity at any given time. If the unstable mode is carefully watched and never allowed to exceed a given threshold, the satellite will remain very close to the desired periodic orbit as long as the threshold is low enough. It has also been shown that for the unperturbed case, this form of control is very inexpensive in terms of total maneuvering fuel expended. The optimization of the maneuver itself was superior to optimization of the maneuver epoch in total station-keeping cost. The control cost could be made very low by selection of a smaller threshold. The epoch optimization controller, though, could be more practical, because the maneuvers are nearly constant and occur at regular intervals and could be scheduled and calculated in advance.

V. *Perturbations*

The satellite in the three-body orbit has been controlled (see Chapter IV). If Earth were in a circular orbit about the sun with no moon or other perturbations, our control problem would be solved. It is the purpose of this chapter to introduce the perturbations to the system due to the motion of the moon about the Earth (we will call this effect "moon"), and the eccentricity of the Earth's orbit about the sun (which we will call "e" or "eccentricity"). Once these perturbations are added, the periodic nature of the orbit may no longer exist even in theory. It is hypothesised, however, that motion very near the three-body orbit will still be at least quasi-periodic and that the application of modal control will stabilise the satellite.

5.1 The Perturbed System

Let us return to the Hamiltonian for the system. Without rewriting it, we note that it can be expanded as a Taylor's series about the periodic orbit (*ie*, $X = X_p$ or $\delta x = 0$). Note that this is not a McLaurin series even though $\delta x = 0$.

$$H(X) = H_0 + H_1 + H_2 + \mathcal{O}(\delta x^3) \tag{5.1}$$

where

$$\begin{aligned} H_0 &= H(X_p) \\ H_1 &= \sum_{\mu=1}^{6} \frac{\partial H}{\partial x_\mu}|_{\delta x=0} \delta x_\mu \\ H_2 &= \frac{1}{2!} \sum_{\mu=1}^{6} \sum_{\nu=1}^{6} \frac{\partial^2 H}{\partial x_\mu \partial x_\nu}|_{\delta x=0} \delta x_\mu \delta x_\nu \end{aligned} \tag{5.2}$$

The first term, H_0, is a scalar constant because it is the value of the Hamiltonian for the periodic orbit; H_1 is identically zero because it describes the motion of the periodic trajectory with respect to itself; H_2 is the quadratic term and is the portion which provided the unperturbed problem discussed in this thesis so far (the Floquet

problem, which is a linear system in the modal variables). There are perturbing forces out there, and in order to find their effects on the system, we must begin again with the statement of the new problem. When we have stated it (see section 5.2), and extracted its mathematics, it will be seen that the perturbations can be represented by a Hamiltonian of their own (H_{pert}) and that we can add their effects to the system by adding in the perturbing Hamiltonian.

$$H = H_0 + H_1 + H_2 + \mathcal{O}(\delta x^3) + H_{pert} \tag{5.3}$$

Recall from Eqs. 2.29 and 2.34 that we have already accounted for the second order term in Eq. 5.1.

$$\delta \dot{x} = A(t)\delta x = Z\frac{\partial H_2}{\partial \delta x}\delta x \tag{5.4}$$

We made the assumption that that the third order term was smaller than the perturbations so we solved the following problem.

$$\delta \dot{x} = Z\frac{\partial H_2}{\partial \delta x}\delta x + Z\frac{\partial H_{pert}}{\partial x} \tag{5.5}$$

It may not be clear yet, but this is a first order linear ODE with a forcing function. We would like to write the problem in the modal variables for simplification so we take the transformation to modal variables from section 3.1.

$$\delta x(t) = F(t)\eta(t) \tag{5.6}$$

Taking the time derivative yields

$$\delta \dot{x}(t) = \dot{F}(t)\eta(t) + F(t)\dot{\eta}(t). \tag{5.7}$$

Now combining Eqs. 5.4, 5.5 and 5.7 we have

$$\dot{F}(t)\eta(t) + F(t)\dot{\eta}(t) = A(t)\delta x + Z\frac{\partial H_{part}}{\partial x} \tag{5.8}$$

Now we substitute for the modal variables and solve for a differential equation in $\dot{\eta}$ (let us also drop the time index).

$$\dot{\eta} = F^{-1}(AF - \dot{F})\eta + F^{-1}Z\frac{\partial H_{part}}{\partial x} \tag{5.9}$$

Recalling Eq. 2.40

$$\dot{F} = AF - FJ \tag{5.10}$$

and solving for J

$$J = F^{-1}(AF - \dot{F}) \tag{5.11}$$

we see we can simplify Eq. 5.9 as follows

$$\dot{\eta} = J\eta + F^{-1}Z\frac{\partial H_{part}}{\partial x} \tag{5.12}$$

It is now easier to see that this is a first order linear ODE with a forcing function.

The control problem that was solved in Chapter IV could have been represented as a linear system. The equations of motion for the system controlled can be written in the modal variables as

$$\dot{\vec{\eta}}(t) = J\vec{\eta}(t) \tag{5.13}$$

This is a linear, constant coefficient set of homogeneous differential equations (remember that this system resulted from analysis of a linear time-periodic system in the state variables). In the perturbed system, we add a forcing function, which forces the solution to be the sum of the homogeneous and particular solutions. The system

remains linear.

$$\dot{\vec{\eta}}(t) = J\vec{\eta}(t) + F^{-1}Z\frac{\partial H_{part}}{\partial x} \tag{5.14}$$

The particular solution has the form (5: 255)

$$\vec{\eta}_p(t) = e^{Jt}\eta_p(t_0) + \int_{t_0}^{t} e^{J(t-\tau)}B(\tau)d\tau \tag{5.15}$$

but we do not need the solution. We need a statement of the differential equations to allow our numerical integrator to calculate the solution over a given time interval. In order to write the differential equations, we need an expression for $B(t) = F^{-1}Z\frac{\partial H_{part}}{\partial x}$. The next section will introduce the problem.

5.2 The Elliptic Restricted Problem

The Restricted Problem of Three Bodies has several modifications. As Ssebehely put it

> The motion of the primaries must satisfy the differential equations governing the dynamics of two gravitational bodies. Consequently the primaries might describe elliptic, parabolic or hyperbolic orbits. The special case of circular motion is [the restricted three-body problem]. Its simplest generalisation, when the primaries describe elliptic orbits . . . is not trivial since its consequences are [that the Hamiltonian will be a function of time](7: 587).

It is the purpose of this section to introduce the method by which we obtained the Hamiltonian and Hamilton's equations of motion for the perturbations introduced by the fact that the Earth's orbit has an eccentricity of about 0.0167. The next section will discuss the added effect of the moon which orbits the Earth with a frequency of about once every 29.53 days (sidereal). Figure 5.1 shows the setup for the elliptic problem where the center of mass symbol on the left indicates the Earth-moon barycenter. The distance from the sun to the Earth-moon barycenter is no longer constant, and is represented by r (not to be confused with $\vec{r}$). Brouwer and Clemence (1: 76) give the expansion for this distance in small eccentricity, e. To

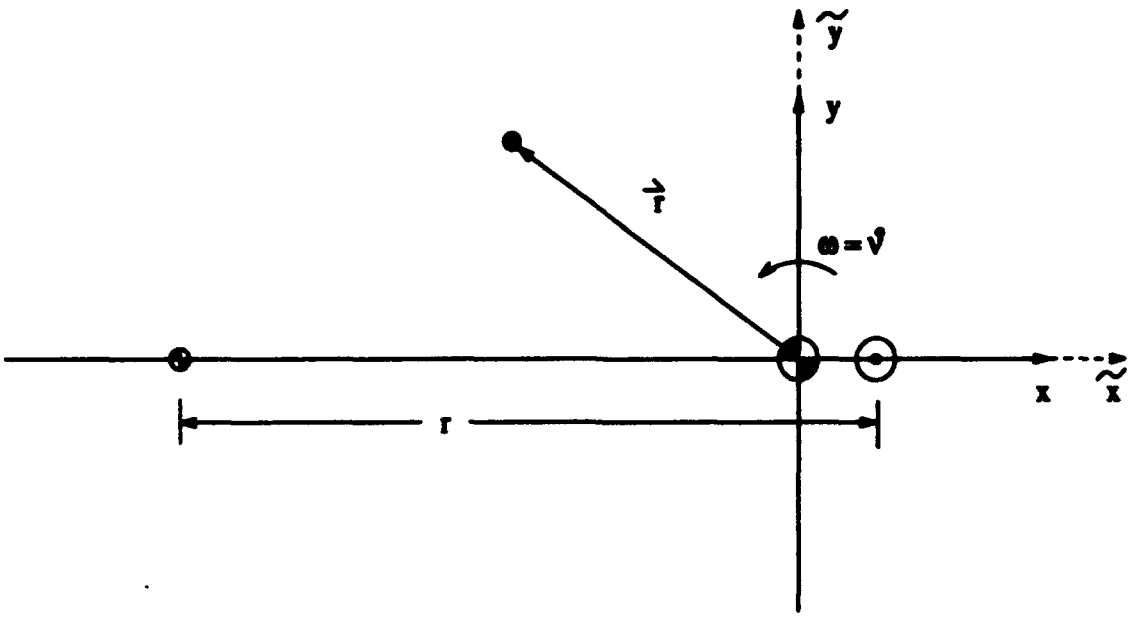

Figure 5.1. The Elliptic Restricted Problem

first order it is

$$r = a(1 - e\cos M) + O(e^2). \tag{5.16}$$

We take a, the semi-major axis, to be 1 AU, the same as before. M is the mean anomaly ($M = n(t - t_0)$) where the mean motion, n, is equal to 1, so that M is equivalent to t. Note that the angular velocity of the rotating reference frame is no longer constant. We denote $\vec{\omega} = \dot{\nu}\hat{k}$. Writing to first order from the expansion for true anomaly, ν (1: 76),

$$\nu = M + 2e\sin M + O(e^2) \tag{5.17}$$

Taking the time derivative yields

$$\omega = \dot{\nu} = n + 2en\cos M + O(e^2) \tag{5.18}$$

We choose coordinates, $\tilde{x}, \tilde{y}, \tilde{z}$ that are scaled by the distance between the Earth and the sun.

$$\begin{aligned} \tilde{x} &= x/r \\ \tilde{y} &= y/r \\ \tilde{z} &= z/r \end{aligned} \tag{5.19}$$

Solving for the spatial coordinates and substituting from Eq. 5.16 for the value of r yields

$$\begin{aligned} x &= \tilde{x}(1 - e\cos t) \\ y &= \tilde{y}(1 - e\cos t) \\ z &= \tilde{z}(1 - e\cos t) \end{aligned} \tag{5.20}$$

and taking derivatives with respect to time,

$$\begin{aligned} \dot{x} &= \dot{\tilde{x}}(1 - e\cos t) + e\tilde{x}\sin t \\ \dot{y} &= \dot{\tilde{y}}(1 - e\cos t) + e\tilde{y}\sin t \\ \dot{z} &= \dot{\tilde{z}}(1 - e\cos t) + e\tilde{z}\sin t. \end{aligned} \tag{5.21}$$

The procedure to follow when writing equations in scaled coordinates is to write them in spatial coordinates first and then transform into the scaled coordinates using equations 5.20 and 5.21. The position vector is as before

$$\vec{r} = x\hat{\imath} + y\hat{\jmath} + z\hat{k} \tag{5.22}$$

in rotating spatial (not scaled) coordinates. Taking the inertial time derivative gives the inertial velocity

$$\vec{v} = (\dot{x} - y - 2ey\cos t)\hat{\imath} + (\dot{y} + x + 2ex\cos t)\hat{\jmath} + \dot{z}\hat{k} + \mathcal{O}(e^2). \tag{5.23}$$

The inertial velocity can then be written in terms of the new coordinates

$$\vec{v} = \begin{pmatrix} \dot{\tilde{x}}(1-e\cos t) + e\tilde{x}\sin t - \tilde{y}(1-e\cos t) - 2e\tilde{y}\cos t) \\ \dot{\tilde{y}} + e\tilde{y}\sin t + \tilde{x}(1-e\cos t) + 2e\tilde{x}\cos t) \\ \dot{\tilde{z}}(1-e\cos t) \end{pmatrix} + \mathcal{O}(e^2). \qquad (5.24)$$

Continuing in the same manner as developed in Chapter II we calculate the kinetic energy, T.

$$\begin{aligned} T &= \tfrac{1}{2}[(\dot{\tilde{x}} - \tilde{y} - e\tilde{y}\cos t - e\dot{\tilde{x}}\cos t + e\tilde{x}\sin t)^2 \\ &+ (\dot{\tilde{y}} + \tilde{x} + e\tilde{x}\cos t - e\dot{\tilde{y}}\cos t + e\tilde{y}\sin t)^2 \\ &+ (\dot{\tilde{z}} - e\dot{\tilde{z}}\cos t)^2] + \mathcal{O}(e^2) \end{aligned} \qquad (5.25)$$

The generalized momenta can be obtained from $p_i = \dfrac{\partial T}{\partial \dot{q}_i}$

$$p_{\tilde{x}} = \frac{\partial T}{\partial \dot{\tilde{x}}} \approx (\dot{\tilde{x}} - \tilde{y} - e\tilde{y}\cos t - e\dot{\tilde{x}}\cos t + e\tilde{x}\sin t)(1-e\cos t) \qquad (5.26)$$

$$p_{\tilde{y}} = \frac{\partial T}{\partial \dot{\tilde{y}}} \approx (\dot{\tilde{y}} + \tilde{x} + e\tilde{x}\cos t - e\dot{\tilde{y}}\cos t + e\tilde{y}\sin t)(1-e\cos t) \qquad (5.27)$$

$$p_{\tilde{z}} = \frac{\partial T}{\partial \dot{\tilde{z}}} \approx (\dot{\tilde{z}} - e\dot{\tilde{z}}\cos t)(1-e\cos t) \qquad (5.28)$$

which are *not* the components of the inertial velocity vector. Now note that after some algebra the kinetic energy can also be written

$$T = \frac{1}{2}\left[\frac{p_{\tilde{x}}^2}{(1-e\cos t)^2} + \frac{p_{\tilde{y}}^2}{(1-e\cos t)^2} + \frac{p_{\tilde{z}}^2}{(1-e\cos t)^2}\right]. \qquad (5.29)$$

This relation will prove useful. It will also be useful to solve for the $\dot{q}_i's$.

$$\begin{aligned} \dot{\tilde{x}} &= \frac{p_{\tilde{x}}}{(1-e\cos t)^2} + \frac{\tilde{y} + e\tilde{y}\cos t - e\tilde{x}\sin t)}{(1-e\cos t)} \\ \dot{\tilde{y}} &= \frac{p_{\tilde{y}}}{(1-e\cos t)^2} - \frac{\tilde{x} + e\tilde{x}\cos t - e\tilde{y}\sin t)}{(1-e\cos t)} \\ \dot{\tilde{z}} &= \frac{p_{\tilde{z}}}{(1-e\cos t)^2} \end{aligned} \qquad (5.30)$$

When it is realized that

$$(1 - e\cos t)^{-2} = 1 + 2e\cos t + \mathcal{O}(e^2) \tag{5.31}$$

and

$$(1 - e\cos t)^{-1} = 1 + e\cos t + \mathcal{O}(e^2) \tag{5.32}$$

then the $\dot{q}_i's$ can be written

$$\begin{aligned} \dot{\tilde{x}} &= p_{\tilde{x}} + \tilde{y} + 2e\tilde{y}\cos t + 2ep_{\tilde{x}}\cos t - e\tilde{x}\sin t \\ \dot{\tilde{y}} &= p_{\tilde{y}} - \tilde{x} + 2e\tilde{x}\cos t + 2ep_{\tilde{y}}\cos t - e\tilde{y}\sin t \\ \dot{\tilde{z}} &= p_{\tilde{z}} + 2ep_{\tilde{z}}\cos t \end{aligned} \tag{5.33}$$

The Hamiltonian for this problem can now be written even though the potentials have not yet been calculated.

$$\begin{aligned} H &= \tfrac{1}{2}(p_{\tilde{x}}^2 + p_{\tilde{y}}^2 + p_{\tilde{z}}^2) + p_{\tilde{x}}\tilde{y} - p_{\tilde{y}}\tilde{x} + V_{rp} \\ &+ ep_{\tilde{x}}^2\cos t + ep_{\tilde{y}}^2\cos t + ep_{\tilde{z}}^2\cos t \\ &+ 2ep_{\tilde{x}}\tilde{y}\cos t - 2ep_{\tilde{y}}\tilde{x}\cos t - ep_{\tilde{x}}\tilde{x}\cos t - ep_{\tilde{y}}\tilde{y}\cos t + V_{pert} \end{aligned} \tag{5.34}$$

The first line of Eq. 5.34 is the same as in Chapter II. It is the "restricted problem" Hamiltonian, H_{rp}. The rest of the Hamiltonian is due entirely to the perturbations. We will write Hamilton's equations of motion after the potentials have been found.

5.3 The Elliptic Four Body Problem

Imagine now that the moon orbits the Earth in a circular orbit in the plane of the ecliptic and that their barycenter orbits the sun in a slightly eccentric orbit. A graphic representation of the problem can be seen in Figure 5.2. This introduces another perturbation arising from the moon's monthly circuit of the Earth. The potentials are affected by this motion of the moon, but the kinetic energy part of the Hamiltonian is not. In order to write the potentials for this problem, we draw

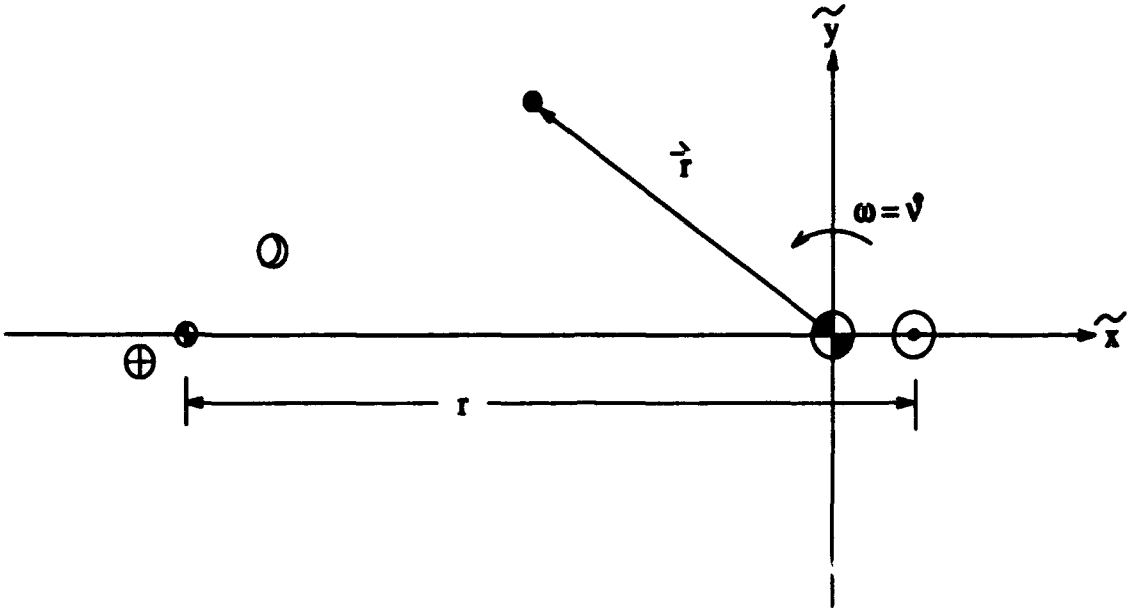

Figure 5.2. Frame of Reference for the Restricted Four Body Problem

another picture. Figure 5.3 shows the vectors to the satellite from each of the three primary bodies, as well as some other pertinent distances. The angular frequency of the moon is $\omega_{\oslash}$. The potential for the satellite is written

$$\begin{aligned} V &= V_{\odot} + V_{\oplus} + V_{\oslash} \\ &= -\frac{m_{\odot}}{r_{\odot,3}} - \frac{m_{\oplus}}{r_{\oplus,3}} - \frac{m_{\oslash}}{r_{\oslash,3}}. \end{aligned} \tag{5.35}$$

where the subscripts denote the body from which the potential originates: $\odot$ is the sun, $\oplus$ is the Earth, and $\oslash$ is the moon. The masses need to be parameterized to keep the units consistent, so we define several $\mu's$ to represent them. These are not to be confused with the original μ for the three-body problem, though they are similar.

$$\begin{aligned} \mu_{\oplus} &= \frac{m_{\oplus}}{m_{\odot} + m_{\oplus} + m_{\oslash}} &&= 3.00348058 \times 10^{-6} \\ \mu_{\odot} &= \frac{m_{\odot}}{m_{\odot} + m_{\oplus} + m_{\oslash}} &&= 3.69429133 \times 10^{-8} \\ \mu_{2} &= \frac{m_{\oslash}}{m_{\oplus} + m_{\oslash}} &&= 1.21505814 \times 10^{-2} \end{aligned} \tag{5.36}$$

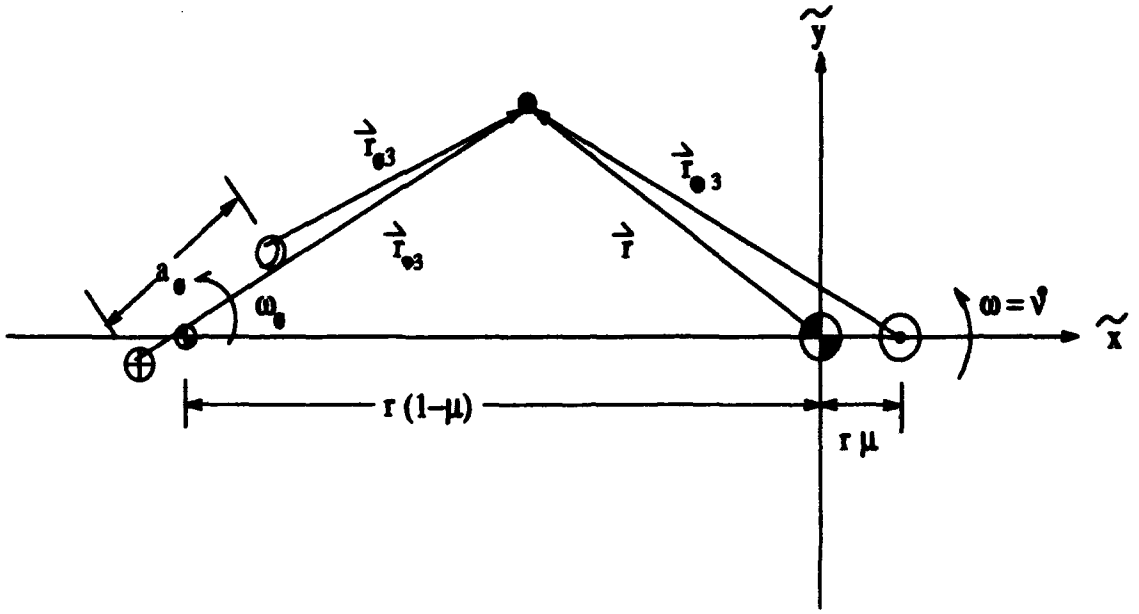

Figure 5.3. More Detail on the Restricted Four Body Problem

The quantity μ_2 is the parameter for the three body problem involving the Earth and moon as primaries.

In order to separate the perturbed Hamiltonian from the rest of the Hamiltonian, it will be necessary to expand the distances in the denominators of the potential in the small parameters (eccentricity of Earth's orbit, e, and the semimajor axis of the moon's orbit, $a_\odot$). We will follow this process closely for the first term (the sun's potential) and the other terms (Earth's and moon's potentials) will be derived in less detail. We are careful to write the vectors in spatial coordinates first and then transform them into scaled coordinates.

$$\vec{r}_{\odot,3} = (x - \mu r)\hat{i} + y\hat{j} + z\hat{k} \tag{5.37}$$

$$= [x - (1 - e\cos t)\mu]\,\hat{i} + y\hat{j} + z\hat{k} + \mathcal{O}(e^2) \tag{5.38}$$

We are expanding its magnitude in the denominator, so we write

$$\frac{1}{|\vec{r}_\odot|} = r_{\odot,3}^{-1} = \left[(x-\mu+\mu e\cos t)^2 + y^2 + z^2\right]^{-\frac{1}{2}} + \mathcal{O}(e^2) \tag{5.39}$$

Now we convert to scaled coordinates.

$$r_{\odot,3}^{-1} = \left[(\tilde{x}-\tilde{x}e\cos t-\mu+\mu e\cos t)^2 + (\tilde{y}(1-e\cos t))^2 + (\tilde{z}(1-e\cos t))^2\right]^{-\frac{1}{2}} + \mathcal{O}(e^2) \tag{5.40}$$

Simplifying, and grouping the large terms from the small ones gives

$$\begin{aligned} r_{\odot,3}^{-1} &= [(\tilde{x}-\mu)^2 + \tilde{y}^2 + \tilde{z}^2 \\ &- 2e(\tilde{x}-\mu)^2\cos t - 2e\tilde{y}^2\cos t - 2e\tilde{z}^2\cos t]^{-\frac{1}{2}} + \mathcal{O}(e^2) \end{aligned} \tag{5.41}$$

Now we expand to first order using a binomial expansion to obtain

$$\begin{aligned} r_{\odot,3}^{-1} &= [(\tilde{x}-\mu)^2 + \tilde{y}^2 + \tilde{z}^2]^{-\frac{1}{2}} \\ &- \tfrac{1}{2}[(\tilde{x}-\mu)^2 + \tilde{y}^2 + \tilde{z}^2]^{-\frac{3}{2}} \\ &\times 2e\cos t(-(\tilde{x}-\mu)^2 - \tilde{y}^2 - \tilde{z}^2) + \mathcal{O}(e^2) \end{aligned} \tag{5.42}$$

which can be simplified greatly by letting $\rho_1 = \sqrt{(\tilde{x}-\mu)^2 + \tilde{y}^2 + \tilde{z}^2}$ (as in Eq. 2.5) so that

$$r_{\odot,3}^{-1} = \frac{1}{\rho_1} + \frac{e\cos t}{\rho_1} \tag{5.43}$$

Now we have an expression for the first term of Eq. 5.35; noting that the mass of the sun is $(1-\mu)$ we have

$$V_\odot = -\frac{(1-\mu)}{\rho_1} - \frac{(1-\mu)e\cos t}{\rho_1} \tag{5.44}$$

$$= V_{\odot rp} + V_{\odot pert} \tag{5.45}$$

where the subscript *rp* denotes the restricted problem (RTBP) and *pert* denotes "perturbed" so that the potential is the sum of the potential due to the three body

problem and the potential due to perturbations. For the sun potential, eccentricity is the only perturbation, so $a_\odot$ does not appear.

The potentials due to the Earth and moon can be solved in a similar way. The vectors to the satellite from the Earth and moon in spatial coordinates are

$$\begin{aligned}
\vec{r}_{\oplus,3} &= [x + (1-\mu)(1 - e\cos t) + a_\odot \mu_2 \cos(\omega_\odot t)]\,\hat{i} \\
&\quad + [y + a_\odot \mu_2 \sin(\omega_\odot t)]\,\hat{j} + z\hat{k} \\
\vec{r}_{\odot,3} &= [x + (1-\mu)(1 - e\cos t) - a_\odot (1-\mu_2) \cos(\omega_\odot t)]\,\hat{i} \\
&\quad + [y - a_\odot (1-\mu_2) \sin(\omega_\odot t)]\,\hat{j} + z\hat{k}
\end{aligned} \tag{5.46}$$

So the inverse distances are

$$\begin{aligned}
r_{\oplus,3}^{-1} &= \left\{[x + (1-\mu)(1 - e\cos t) + a_\odot \mu_2 \cos(\omega_\odot t)]^2 \right. \\
&\quad \left. + [y + a_\odot \mu_2 \sin(\omega_\odot t)]^2 + z^2 \right\}^{-\frac{1}{2}} \\
r_{\odot,3}^{-1} &= \left\{[x + (1-\mu)(1 - e\cos t) - a_\odot (1-\mu_2) \cos(\omega_\odot t)]^2 \right. \\
&\quad \left. + [y - a_\odot (1-\mu_2) \sin(\omega_\odot t)]^2 + z^2 \right\}^{-\frac{1}{2}}
\end{aligned} \tag{5.47}$$

We then transform into scaled coordinates from Eq. 5.20 to give

$$\begin{aligned}
r_{\oplus,3}^{-1} &= \left\{[\tilde{x}(1 - e\cos t) + (1-\mu)(1 - e\cos t) + a_\odot \mu_2 \cos(\omega_\odot t)]^2 \right. \\
&\quad \left. + [\tilde{y}(1 - e\cos t) + a_\odot \mu_2 \sin(\omega_\odot t)]^2 + [\tilde{z}(1 - e\cos t)]^2 \right\}^{-\frac{1}{2}} \\
r_{\odot,3}^{-1} &= \left\{[\tilde{x}(1 - e\cos t) + (1-\mu)(1 - e\cos t) - a_\odot (1-\mu_2) \cos(\omega_\odot t)]^2 \right. \\
&\quad \left. + [\tilde{y}(1 - e\cos t) - a_\odot (1-\mu_2) \sin(\omega_\odot t)]^2 + [\tilde{z}(1 - e\cos t)]^2 \right\}^{-\frac{1}{2}}
\end{aligned} \tag{5.48}$$

These are expanded in both e and $a_\odot$, and the second order terms are removed. We again let $\rho_2 = \sqrt{(\tilde{x} + 1 - \mu)^2 + \tilde{y}^2 + \tilde{z}^2}$ and multiply by the respective masses to

obtain

$$\begin{aligned} V_{\odot} &= \frac{-\mu_{\odot}}{\rho_2} + \frac{\mu_{\odot}\beta_1}{\rho_2^3} = V_{\odot rp} + V_{\odot pert} \\ V_{\oplus} &= \frac{-\mu_{\oplus}}{\rho_2} + \frac{\mu_{\oplus}\beta_2}{\rho_2^3} = V_{\oplus rp} + V_{\oplus pert} \end{aligned} \tag{5.49}$$

where the β's are given by

$$\begin{aligned} \beta_1 &= -\rho_2 \cos te + \mu_2 \left[\tilde{y}\sin(\omega_{\odot}t) + (\tilde{x} + 1 - \mu)\cos(\omega_{\odot}t)\right] a_{\odot} \\ \beta_2 &= -\rho_2 \cos te - (1-\mu_2)\left[\tilde{y}\sin(\omega_{\oplus}t) + (\tilde{x} + 1 - \mu)\cos(\omega_{\oplus}t)\right] a_{\oplus}. \end{aligned} \tag{5.50}$$

Again we see that the potentials are the sum of the previous potential and a new perturbation potential.

In order to get equations of motion for the system, we take the derivative of the Hamiltonian with respect to the state vector as described in Chapter II

$$\dot{X} = Z\frac{\partial H}{\partial X} \tag{5.51}$$

Rather than repeat the work listed in Chapter II, we will give the partial derivatives of only the perturbed Hamiltonian, H_p, with respect to the elements of the state vector, where we will let the subscript p denote *perturbed*.

$$\begin{aligned} H_p &= ep_{\tilde{x}}^2 \cos t + ep_{\tilde{y}}^2 \cos t + ep_{\tilde{z}}^2 \cos t + 2ep_{\tilde{x}}\tilde{y}\cos t - 2ep_{\tilde{y}}\tilde{x}\cos t \\ &- ep_{\tilde{x}}\tilde{x}\sin t - ep_{\tilde{y}}\tilde{y}\sin t + V_{\odot p} + V_{\oplus p} + V_{\oplus p} \end{aligned} \tag{5.52}$$

$$
\begin{aligned}
\frac{\partial H_p}{\partial \tilde{x}} &= -2ep_{\tilde{y}}\cos t - ep_{\tilde{x}}\sin t + \frac{\partial V_{\odot p}}{\partial \tilde{x}} + \frac{\partial V_{\oplus p}}{\partial \tilde{x}} + \frac{\partial V_{\oplus p}}{\partial \tilde{x}} \\
\frac{\partial H_p}{\partial \tilde{y}} &= 2ep_{\tilde{x}}\cos t - ep_{\tilde{y}}\sin t + \frac{\partial V_{\odot p}}{\partial \tilde{y}} + \frac{\partial V_{\oplus p}}{\partial \tilde{y}} + \frac{\partial V_{\oplus p}}{\partial \tilde{y}} \\
\frac{\partial H_p}{\partial \tilde{z}} &= \frac{\partial V_{\odot p}}{\partial \tilde{z}} + \frac{\partial V_{\oplus p}}{\partial \tilde{z}} + \frac{\partial V_{\oplus p}}{\partial \tilde{z}} \\
\frac{\partial H_p}{\partial p_{\tilde{x}}} &= 2e\tilde{y}\cos t + 2ep_{\tilde{x}}\cos t - e\tilde{x}\sin t \\
\frac{\partial H_p}{\partial p_{\tilde{y}}} &= -2e\tilde{x}\cos t + 2ep_{\tilde{y}}\cos t - e\tilde{y}\sin t \\
\frac{\partial H_p}{\partial p_{\tilde{z}}} &= 0
\end{aligned}
\tag{5.53}
$$

The partials of the potential terms are given by

$$
\begin{aligned}
\frac{\partial V_{\odot p}}{\partial \tilde{x}} &= \frac{e(\mu - \tilde{x})\cos t}{\rho_1^3}(1-\mu) \\
\frac{\partial V_{\odot p}}{\partial \tilde{y}} &= \frac{e\tilde{y}\cos t}{\rho_1^3}(1-\mu) \\
\frac{\partial V_{\odot p}}{\partial \tilde{z}} &= \frac{e\tilde{z}\cos t}{\rho_1^3}(1-\mu)
\end{aligned}
\tag{5.54}
$$

$$
\begin{aligned}
\frac{\partial V_{\oplus p}}{\partial \tilde{x}} &= \left[\frac{3a_{\odot}\mu_2(\tilde{x}+1-\mu)[(\tilde{x}+1-\mu)\cos(\omega_{\odot}t) + \tilde{y}\sin(\omega_{\odot}t)]}{\rho_2^5}\right. \\
&+ \left.\frac{a_{\odot}\mu_2\cos(\omega_{\odot}t)}{\rho_2^3} - \frac{(\tilde{x}+1-\mu)\cos te}{\rho_2^3}\right]\mu_{\oplus} \\
\frac{\partial V_{\oplus p}}{\partial \tilde{y}} &= \left[\frac{3a_{\odot}\mu_2\tilde{y}[(\tilde{x}+1-\mu)\cos(\omega_{\odot}t) + \tilde{y}\sin(\omega_{\odot}t)]}{\rho_2^5}\right. \\
&+ \left.\frac{a_{\odot}\mu_2\sin(\omega_{\odot}t)}{\rho_2^3} - \frac{\tilde{y}\cos te}{\rho_2^3}\right]\mu_{\oplus} \\
\frac{\partial V_{\oplus p}}{\partial \tilde{z}} &= \left[\frac{3a_{\odot}\mu_2\tilde{z}[(\tilde{x}+1-\mu)\cos(\omega_{\odot}t) + \tilde{y}\sin(\omega_{\odot}t)]}{\rho_2^5} - \frac{\tilde{z}\cos te}{\rho_2^3}\right]\mu_{\oplus}
\end{aligned}
\tag{5.55}
$$

$$
\begin{aligned}
\frac{\partial V_{\odot p}}{\partial \tilde{x}} &= -\left[\frac{3a_{\odot}(1-\mu_2)(\tilde{x}+1-\mu)[(\tilde{x}+1-\mu)\cos(\omega_{\odot}t)+\tilde{y}\sin(\omega_{\odot}t)]}{\rho_2^5}\right. \\
&\quad \left. + \frac{a_{\odot}(1-\mu_2)\cos(\omega_{\odot}t)}{\rho_2^3} - \frac{(\tilde{x}+1-\mu)\cos te}{\rho_2^3}\right]\mu_{\odot} \\
\frac{\partial V_{\odot p}}{\partial \tilde{y}} &= -\left[\frac{3a_{\odot}(1-\mu_2)\tilde{y}[(\tilde{x}+1-\mu)\cos(\omega_{\odot}t)+\tilde{y}\sin(\omega_{\odot}t)]}{\rho_2^5}\right. \\
&\quad \left. + \frac{a_{\odot}(1-\mu_2)\sin(\omega_{\odot}t)}{\rho_2^3} - \frac{\tilde{y}\cos te}{\rho_2^3}\right]\mu_{\odot} \\
\frac{\partial V_{\odot p}}{\partial \tilde{z}} &= -\left[\frac{3a_{\odot}(1-\mu_2)\tilde{y}[(\tilde{x}+1-\mu)\cos(\omega_{\odot}t)+\tilde{y}\sin(\omega_{\odot}t)]}{\rho_2^5} - \frac{\tilde{z}\cos te}{\rho_2^3}\right]\mu_{\odot}
\end{aligned}
\tag{5.56}
$$

We now have our expression for $\frac{\partial H_p}{\partial x}$ in the variational state variables. If we premultiply it by Z and add it to $Z\frac{\partial H}{\partial x}$ we get the right hand side of the total problem (see Eq. 5.5). A premultiplication by F^{-1} will transform the problem into the modal variables (see Eq. 5.12).

The total problem has been stated and the integrator will integrate these equations of motion readily. It should be noted here that the introduction of a forcing function to our linear system creates a particular solution, which is added to the homogeneous solution to form the total. The total solution is the one that is observed, and it is the one whose modes are controlled. The nature of the particular solution, which may have some significance in the control of the satellite, is ignored. It is known that if the unstable mode of the particular solution diverges in one direction (say toward $+\infty$) then the homogeneous solution can be made to diverge in the opposite direction (a very large negative number) so that their sum is quite small. The consequences of this simultaneous divergence during the control of the satellite have not yet been discovered.

VI. Results of Perturbation Controller

The problems associated with the perturbed orbit were many. The periodic orbit no longer existed in the same sense that it did before. The satellite placed near the three-body orbit was able to nearly close on itself several times before diverging (see section 4.1), but the perturbations cause the satellite to diverge much sooner — before completing a single orbit. See Figure 6.1.

6.1 Simplification of System

When perturbations from the eccentricity and the moon were included in the model, the controller failed to adequately control the satellite in the orbit. The reasons for this are not precisely known. Perhaps the second order effects should be taken into account before the mode shapes will be similar enough to the unperturbed case for the controller to be effective. Perhaps the difference between the particular and the homogeneous solutions caused the total solution to compound numerical errors so that the simulation broke down. In any case, the perturbations due to eccentricity were put aside, and the effects of the moon alone were studied. The results shown in this section will be the results of the controller acting upon a simulated system where the earth is in a circular orbit about the sun, but the moon is also in orbit about the earth, and is affecting the satellite with its gravity. The equations of motion and the computer code which integrates them remain exactly the same, with the simple change of setting e equal to zero.

With the simplified system, the modal control scheme was successful. Even with $e = 0$, the uncontrolled satellite diverged before completing a single orbit, but the divergence was somewhat slower. See Figure 6.2. Using modal control, it was kept in the vicinity of the orbit indefinitely as long as the threshold was small enough.

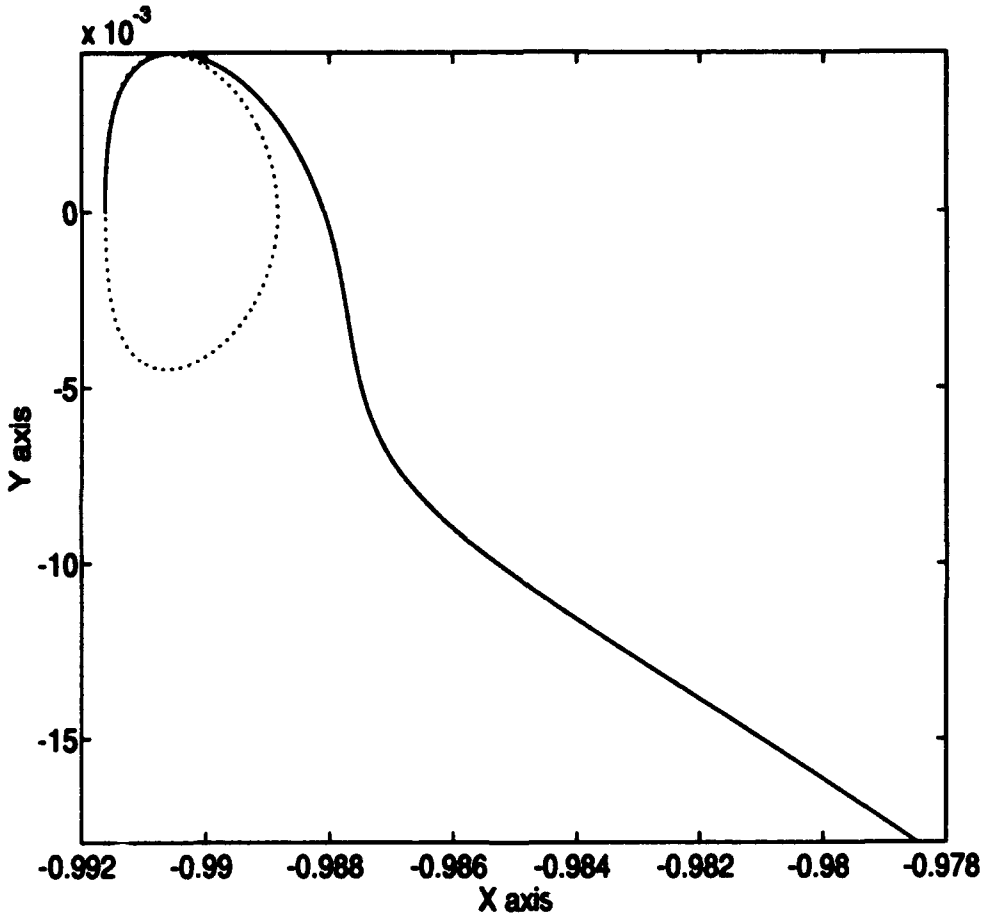

Figure 6.1. X – Y Projection of Satellite Path Diverging Before Completing First Orbit. (.... = Periodic Orbit — = Satellite Path)

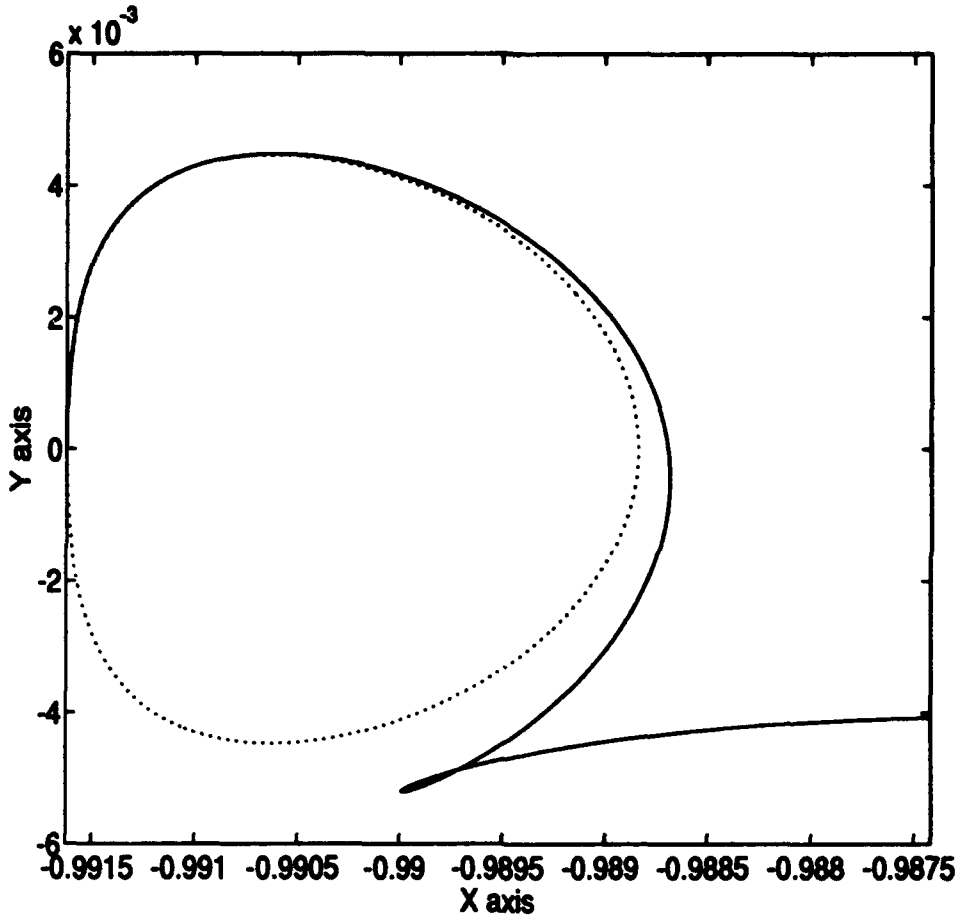

Figure 6.2. X – Y Projection of Satellite Path Diverging Even Without Eccentricity. (.... = Periodic Orbit — = Satellite Path)

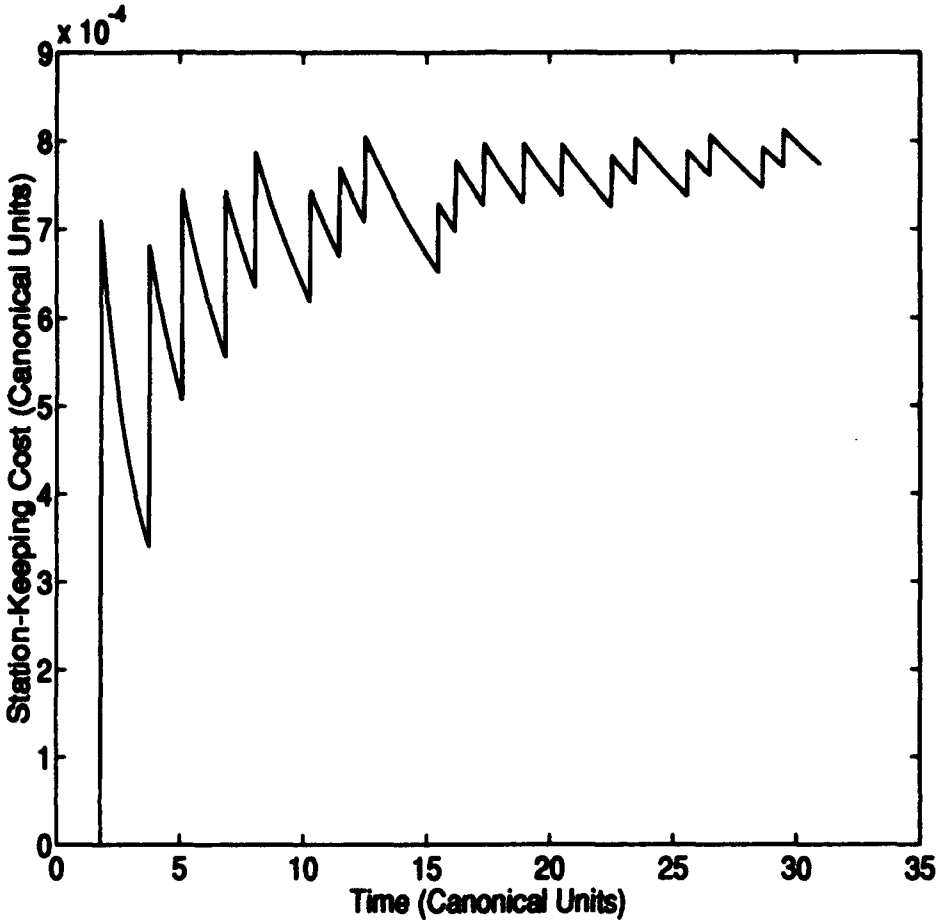

Figure 6.3. Average Station-Keeping Cost for Moon-Perturbed Orbit, Threshold = 10^{-3}

6.2 Results

Let us look first at a threshold which gives a very similar result to the unperturbed case. The threshold in this case was about 10^{-3}. See figures 6.3, 6.4 and 6.5. All the simulations in this section were run for 31 time units (canonical) which is close to 10 orbital periods or about 5 years. The station-keeping cost for this first simulation is very high. When the canonical units are converted to more conventional units, it cost about 200 m/sec per year to control the satellite with this threshold.

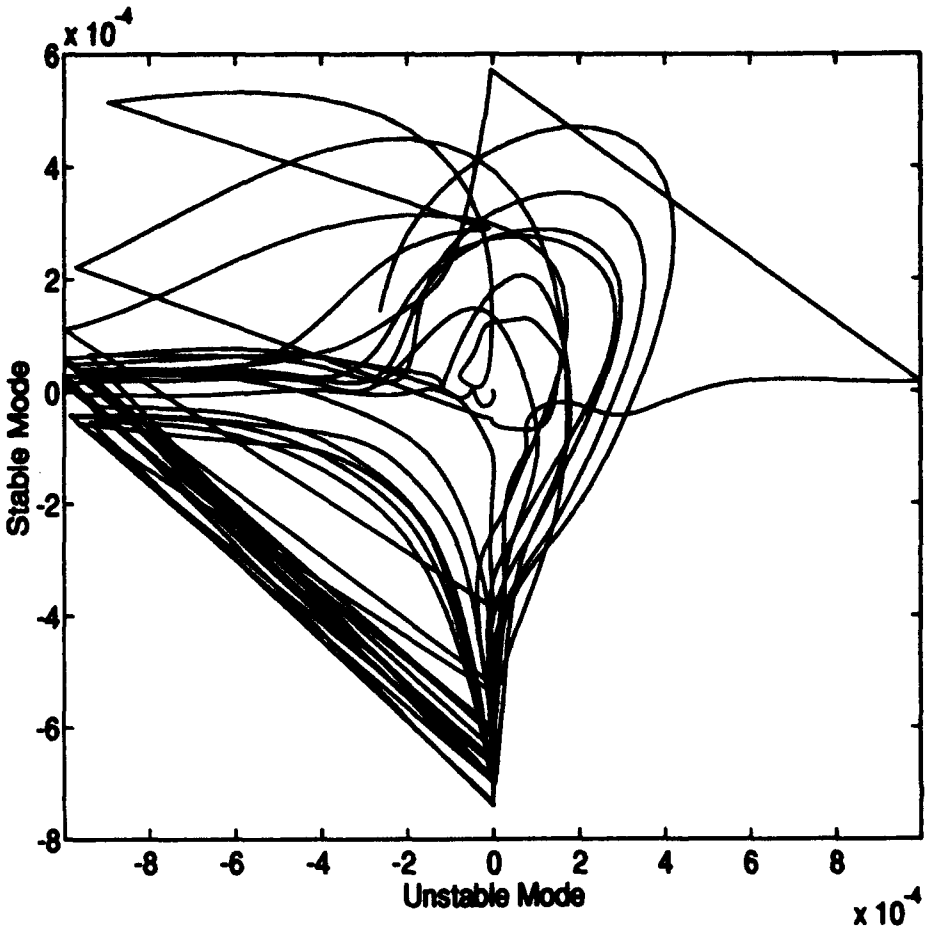

Figure 6.4. Plot of the Real Modes, Threshold = 10^{-3}

The mode shapes for this simulation were somewhat regular (figure 6.4). Even though the maneuvers do not zero out both modes (the stable mode is given a positive value while the unstable mode is set to near zero–just like in section 4.4), the behavior seems to be fairly predictable. There are some funny curves in the plot, and these are due to the perturbations.

Figure 6.5 shows the approximate "Earth view" for the orbit. It is a trace of the Y and Z positions of the satellite throughout the simulation. It shows that there is considerable wobble in the orbit, which may or may not be acceptable depending

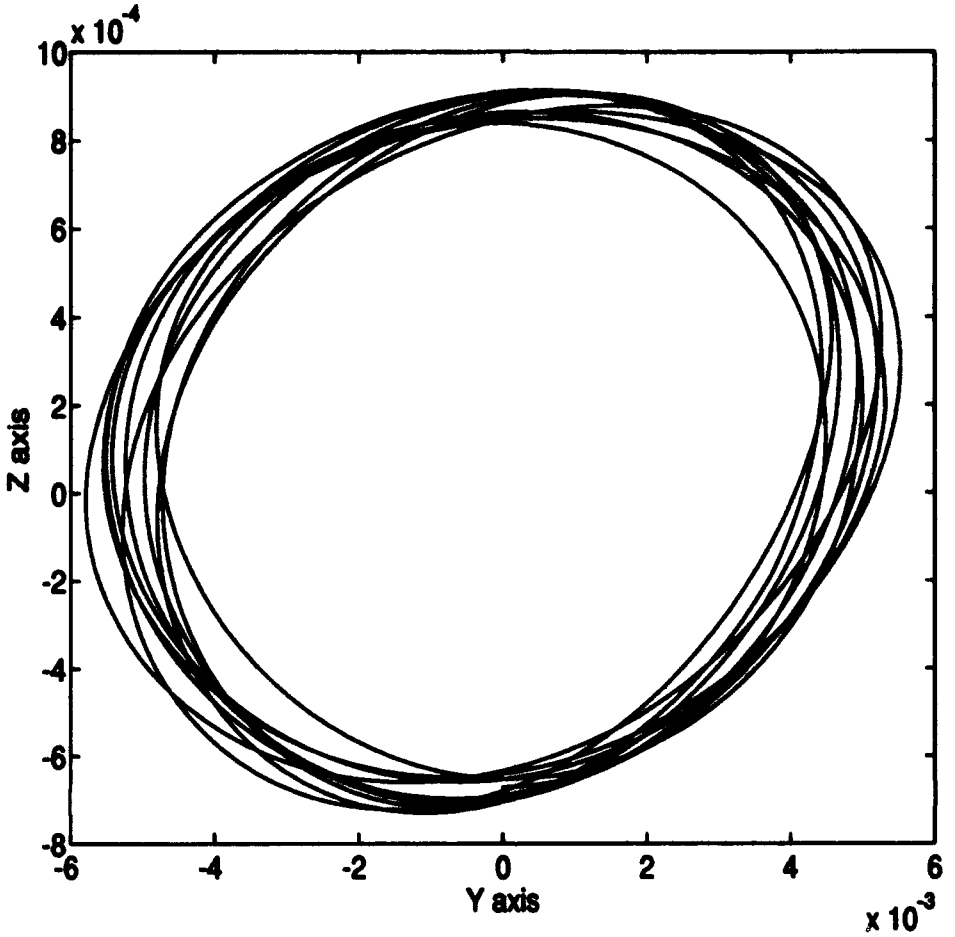

Figure 6.5. Plot of the Y – Z Projection of the Orbit, Threshold = 10^{-3}

on the size of the sun's radio disk and other constraints. Interestingly enough, the orbit is both cheaper to control and more controlled at this threshold than the unperturbed orbit was. Compare to Figure 4.10.

If we decrease the threshold for the unstable mode, we can decrease the control cost somewhat. Figure 6.6 shows the cost for a threshold of 10^{-6}. Although the total average cost is lower for this option (about 20 m/sec per year), it requires very frequent maneuvers. During this simulation, over 300 maneuvers were performed, averaging about 5 per month.

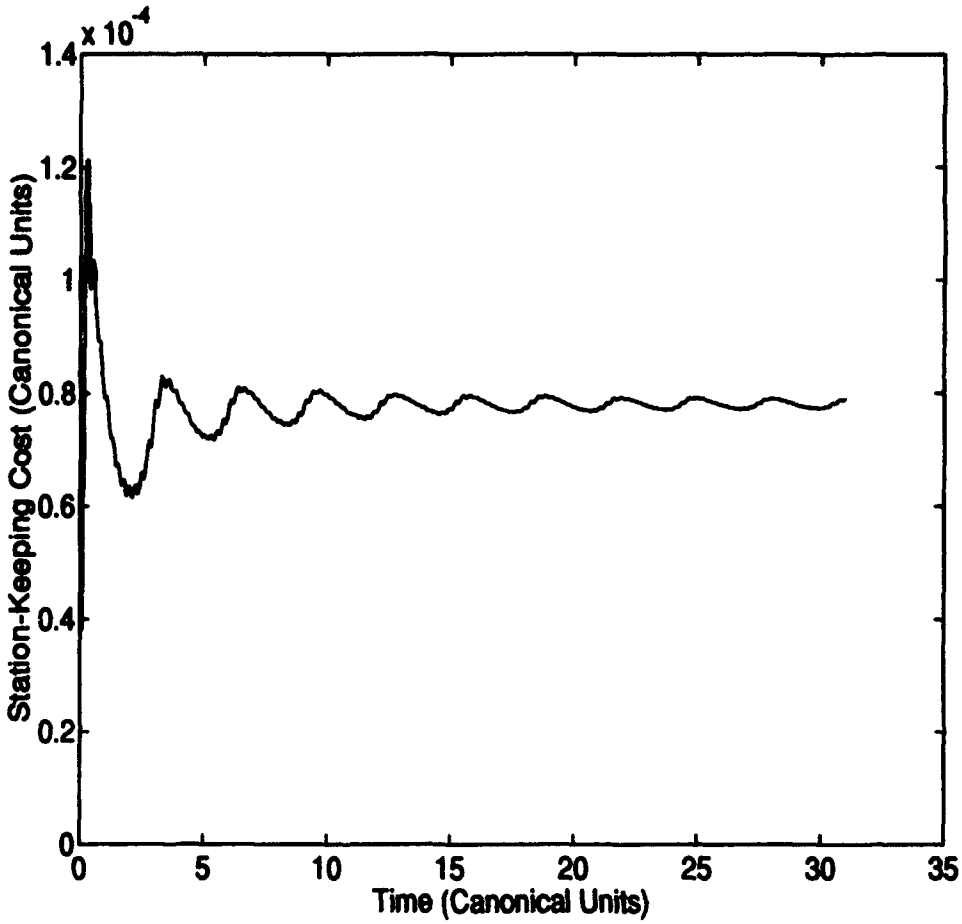

Figure 6.6. Station-Keeping Cost with Threshold = 10^{-6} Showing the Maneuvering is Extremely Frequent.

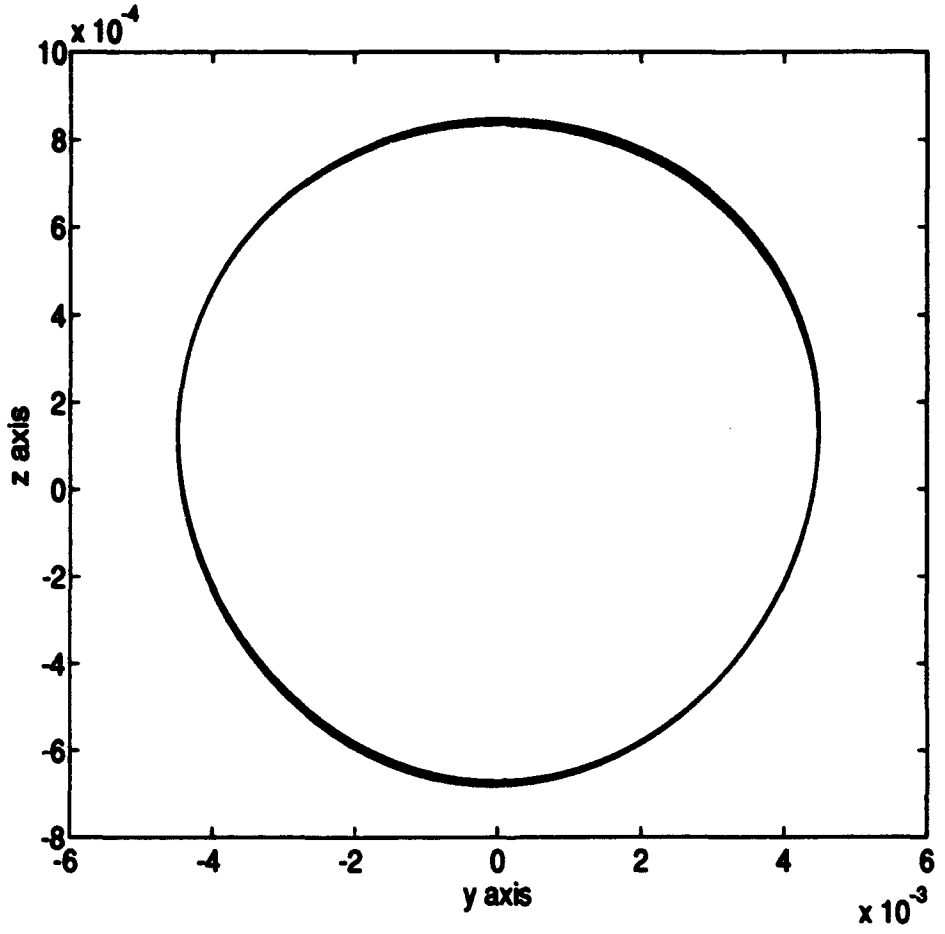

Figure 6.7. Y – Z Projection (Like the View from Earth) of Controlled Satellite's Orbit, Threshold = 10^{-6}

The Y – Z projection of the orbit (see Figure 6.7) shows considerable tightness in the control of the orbit. The slight anomalies that can be seen here are due to the periodic fluctuations in the perturbing force of the moon's gravity and not to divergence and subsequent control of the unstable mode.

Since the manuevers were so frequent with the threshold at 10^{-6}, an attempt was made using trial and error (shall we say, "trial and success") to optimize the threshold to decrease the number of maneuvers required and to decrease the total station-keeping cost if possible. The attempt was successful with a threshold of

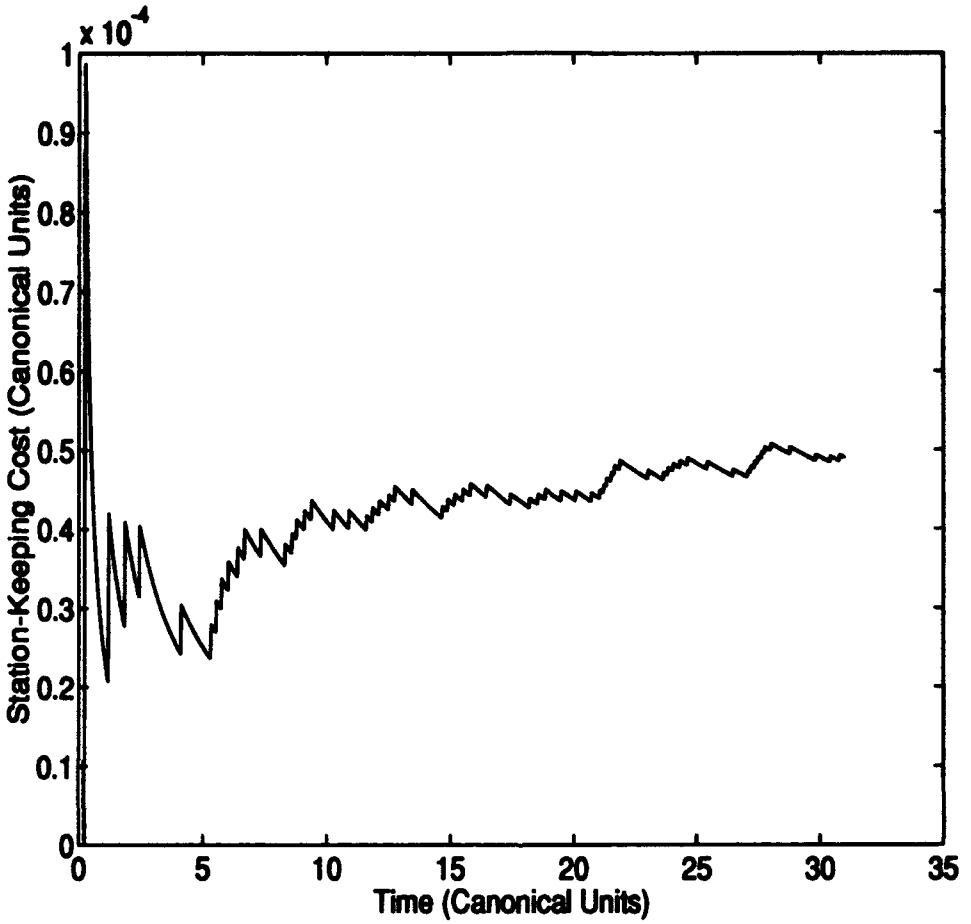

Figure 6.8. Station-Keeping Cost, Threshold = 2×10^{-5}

2×10^{-5}. Figure 6.8 shows the cost, which is about 10 m/sec per year when units are converted. It can also be seen that there are fewer maneuvers — about one per month. The average maneuver was about 72.5 cm/sec.

Figure 6.9 is a plot of the real modes. It seems rather jumbled, but this is because the threshold is on the same order (spatial and temporal frequency) as the gyrations of the modes so that the maneuver occurs in unpredictable positions on the plot. What is important is that the unstable mode never exceeds the threshold, and that it is allowed to "wander" until its wandering begins to diverge.

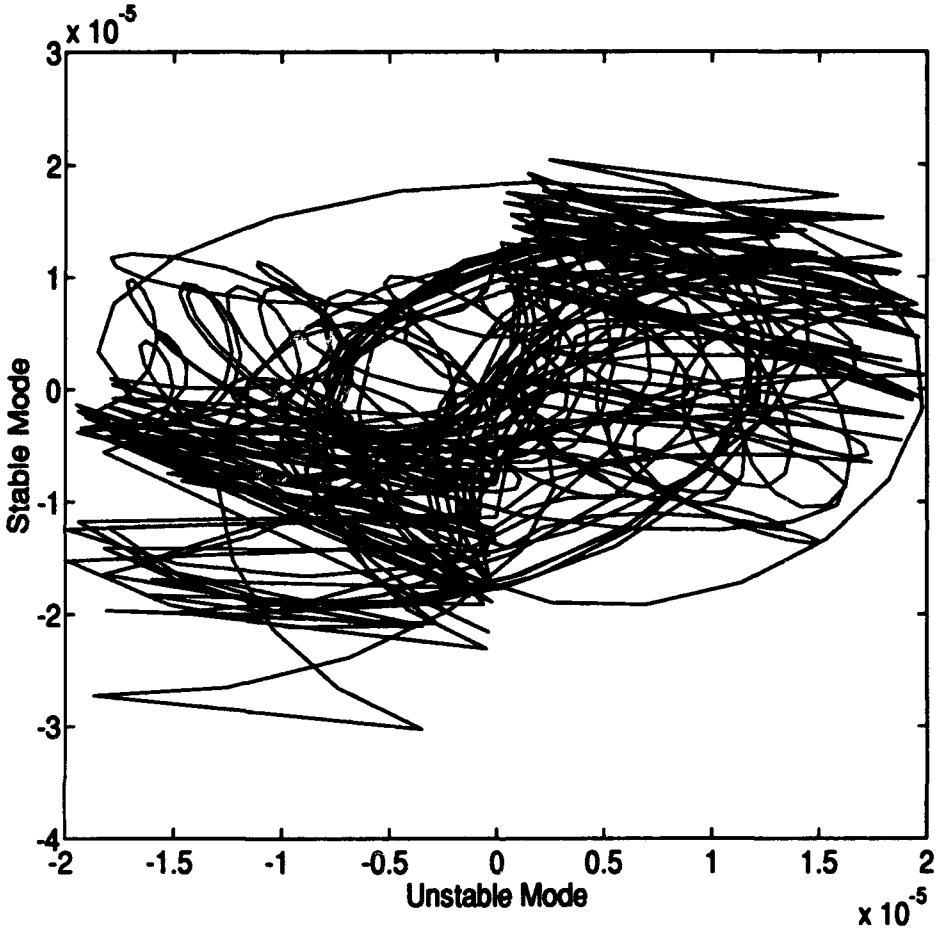

Figure 6.9. Real Modes Under Control for Threshold $= 2 \times 10^{-5}$

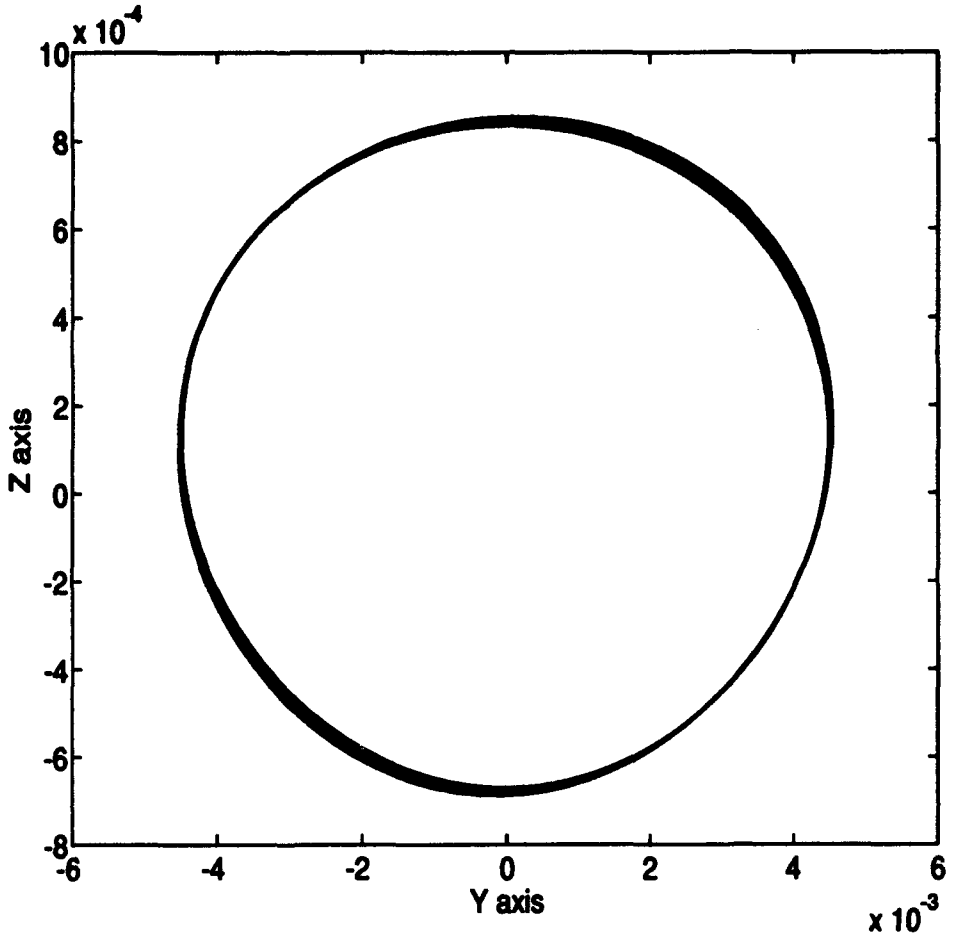

Figure 6.10. Y – Z Projection for the Satellite Path, Threshold $= 2 \times 10^{-5}$

The Earth-view for this threshold shows a very small divergence from the nominal orbit, which would be acceptable under most circumstances. If the path crossed too close to the sun, the best alternative would be to find a new periodic reference orbit in the three-body problem which had larger amplitude rather than attempt tighter control.

Let us look at the cost as a function of the threshold for the perturbed satellite. Figure 6.11 shows the station-keeping cost for a number of different thresholds.

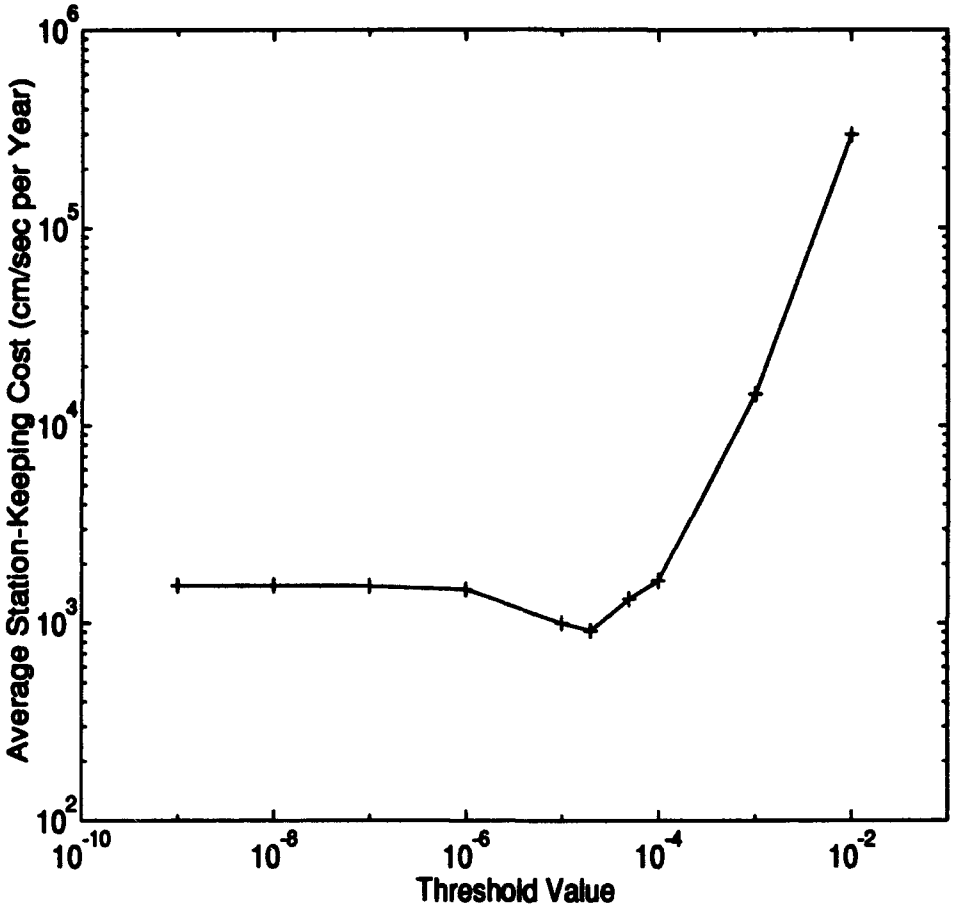

Figure 6.11. Station-Keeping Cost as a Function of Threshold

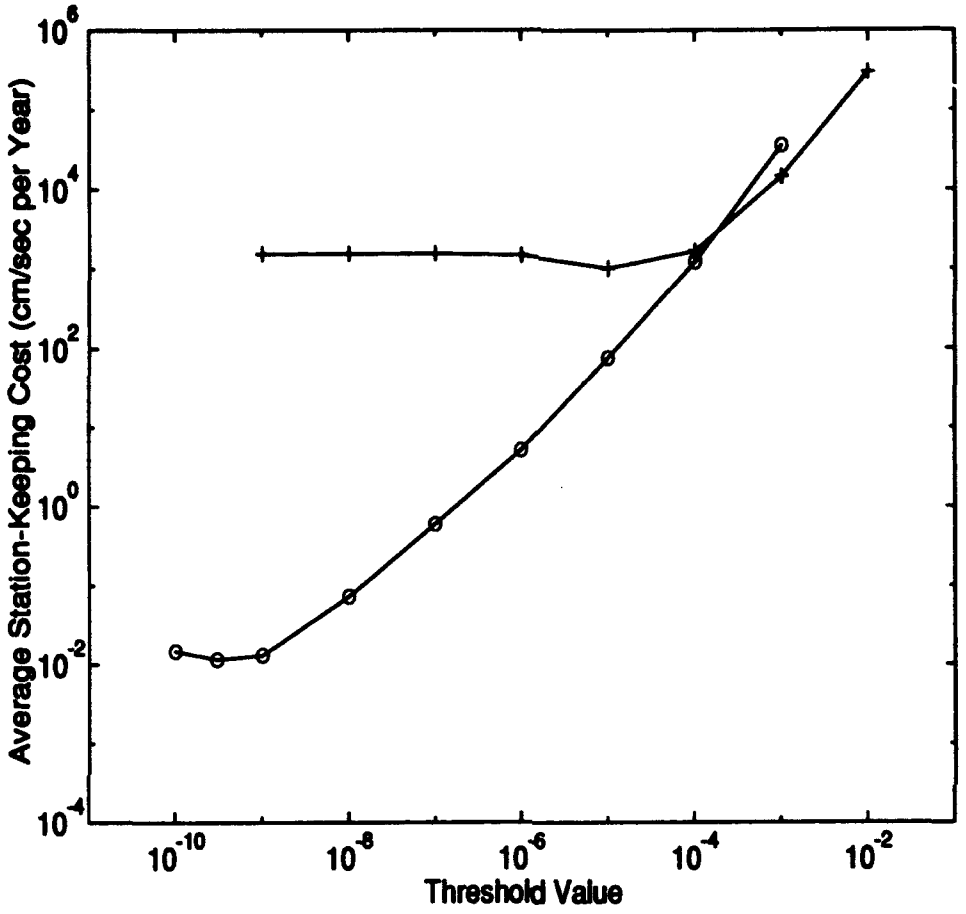

Figure 6.12. Cost Comparison for Perturbed (+) vs Unperturbed (o) Systems

It is easy to see that the perturbed satellite is more expensive to control than the unperturbed satellite by looking at Figure 6.12. When two comparable scenarios are compared (threshold = 10^{-7} for the unperturbed and 2×10^{-5} for the perturbed), we see that the perturbed satellite requires 1000 times more control energy than the unperturbed satellite.

6.3 Behavior of the Other Modes

Once again, the behavior of the other modes under control is interesting and will therefore be included here. The perturbing effect of the moon caused some interesting shapes in them.

Let us look at Figure 6.13. During each of the maneuvers, there is a discontinuity in the plot, plotted with a straight line, but hardly visible on this plot because the manuevers have such small effect on this mode. Between maneuvers, when the satellite is drifting freely, the imaginary modes tend to trace out a skewed 5-pointed star shape, which slowly drifts away from the origin. This is due to the moon's gravity, and as we would expect, the period of the perturbation effects is about six times the period of the orbit. This makes sense since the moon's motion has a period of one month to the halo orbit's six months.

Figure 6.14 is like the previous figure, with the zero modes plotted instead of the imaginary modes. When the satellite is drifting freely, the value of the modes shows the star shape, and when a maneuver is performed, their value changes slightly in some predictable direction, to repeat the figure until the next maneuver.

6.4 Summary

The satellite perturbed by the eccentricity was not controllable with this controller. When the moon only was included, however, the situation improved dramatically. The modes displayed their expected behavior within reason, with some unpredictable perturbation effects. The satellite was controllable with reasonable, if higher, control costs. The reasons for the failure with the eccentricity included are discussed in Chapter VII.

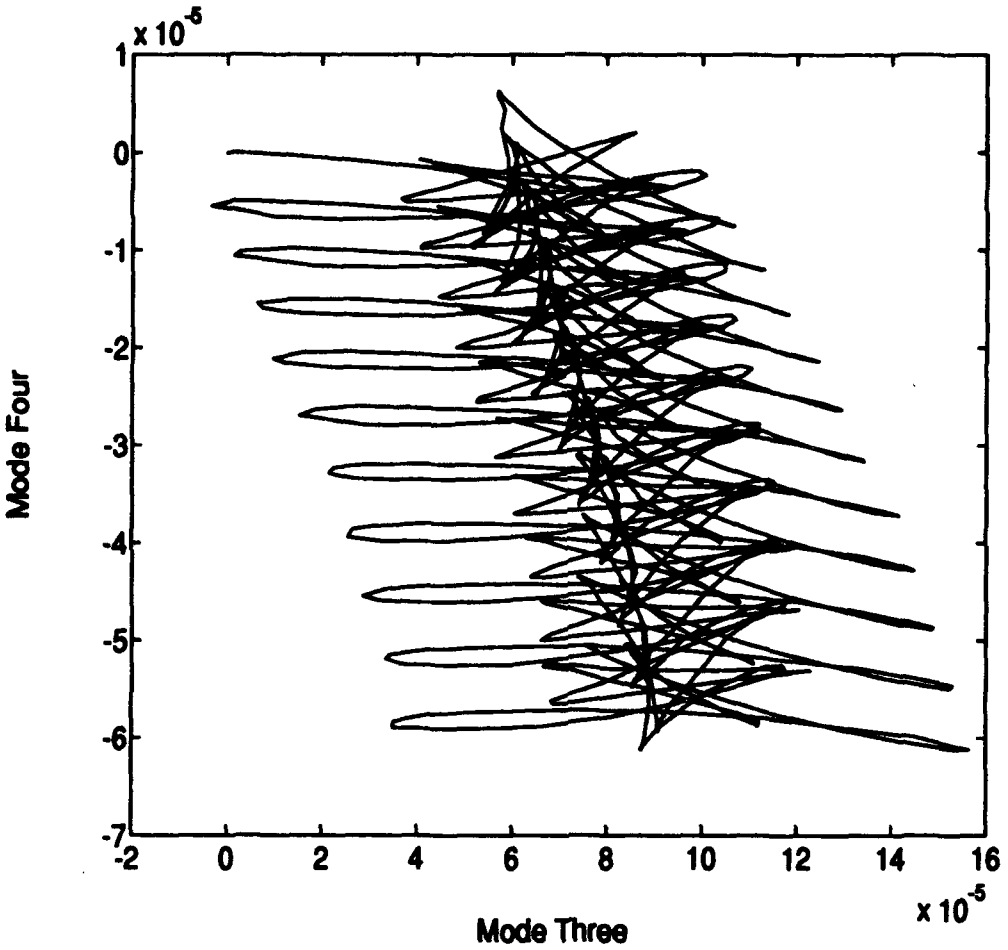

Figure 6.13. Imaginary Modes Plotted Together While Satellite is Under Realistic Control

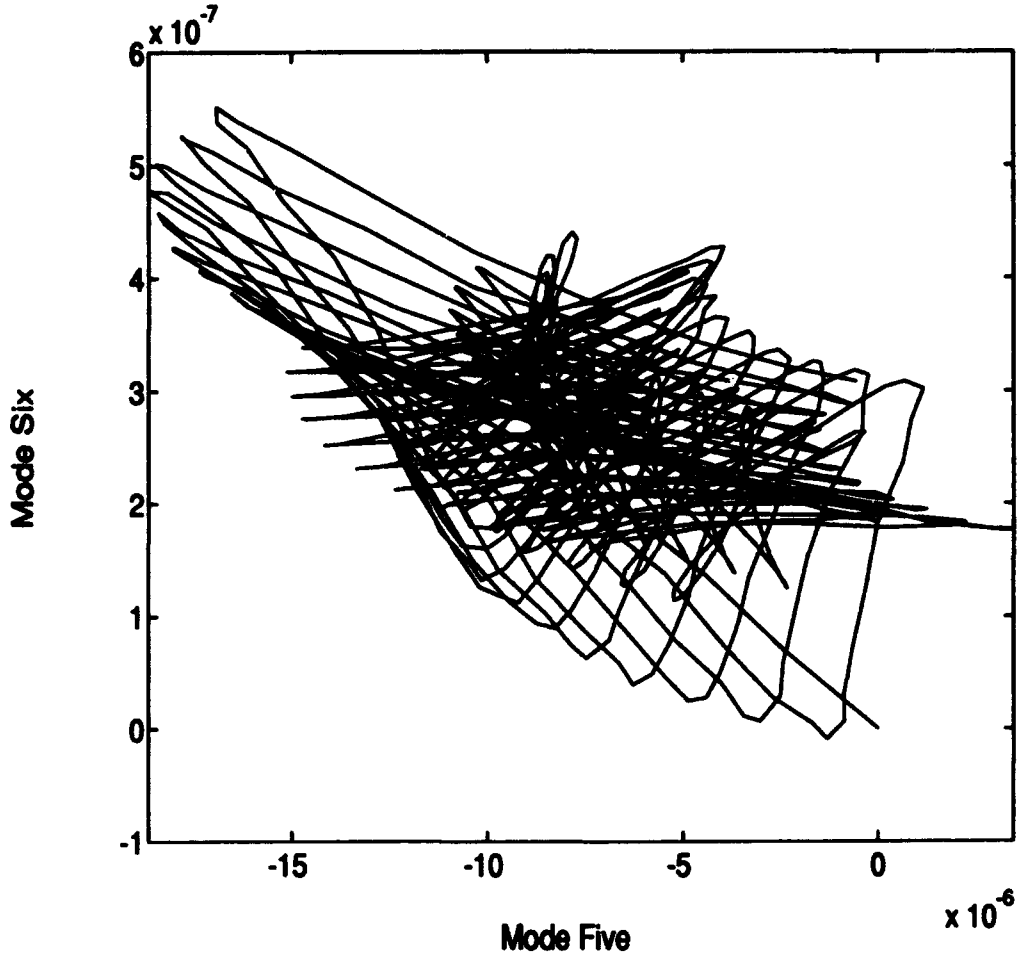

Figure 6.14. Zero Modes Plotted Together While Satellite is Under Realistic Control

VII. Conclusions and Recommendations

7.1 Conclusions

Modal control works well on the unperturbed three-body problem satellite. Using maneuvers calculated by simulated observation of the modes, the satellite was controlled for as long as desired. The concept was simple, and the application was ideal. Modal control held promise of being more efficient than other optimal control algorithms for this type of orbit.

We learned from our cheater controller that each of the modes had a character which depended on its Poincaré exponent. The character was exactly what was expected as long as the magnitude remained small (within the *linear* region). The real exponents corresponded to an exponentially decreasing mode (negative exponent) and an exponentially increasing mode (positive real exponent). The imaginary modes (corresponding to the imaginary exponents) oscillated sinusoidally and were 90 degrees out of phase with each other as indicated by Figure 4.2, where they form a circle when plotted together. The zero modes were static to within reasonable numerical accuracy.

The efficiency of the controller on the unperturbed satellite was improved by decreasing the threshold value up to a point. After that, the cost actually increased when the threshold was decreased. This was due to the numerical inaccuracy of the integration at such small values of the modes (less than 10^{-9}). The station-keeping costs for the unperturbed satellite were phenomenally low. For a 15 year mission, the satellite could be maintained with 1.5 cm/sec of ΔV total (threshold = 10^{-7}) with 2 small maneuvers per year.

The perturbed satellite had a different character. The perturbation due to eccentricity was very large, and very probably pulled the satellite out of the linear region very quickly, which invalidated the shapes of the modes and thus the control scheme. The perturbation due to the moon was not as large, and the modes,

while noticeably different than the unperturbed modes, were still recogniseable. We were not able to decrease the station-keeping cost nearly as much by decreasing the threshold. This makes sense, since decreasing the threshold caused a lot of unnecessary maneuvering. The moon was very quick to pull the satellite off the periodic orbit and thus to cause the modes to grow, but only to a point, and if we maneuvered right away, we missed the fact that the moon just as surely "pushed" the satellite right back near the orbit during the second half of the month. The best strategy was to wait to maneuver when the unstable mode was actually beginning to grow of its own accord, and not due the perturbation. The threshold that worked best for the perturbed satellite was 2×10^{-5}. The station-keeping cost for this threshold was approximately 1 m/sec per year, nearly 3 orders of magnitude higher than the unperturbed cost.

7.2 Recommendations

The perturbations due to eccentricity must be included in any model that represents itself as realistic. There are other perturbations, but they are smaller (2). It is recommended that some scheme for including this perturbation be found, which allows the mode shapes to remain apparent, so that modal control will work. Perhaps a model based on an expansion to second order in the eccentricity would work.

In order to validate the modal control scheme as workable, there must also be studies done on the probabilistic problem of orbit (and thus mode) determination. The halo satellite presents special problems in this area, which have been studied by Howell and Pernicka — see references (3) and (4), but not with modal control.

The consequences of the particular solution divergence while the total solution remains finite have not been addressed. If this scheme is to be workable, the solutions to the mathematical model must be very well understood, so it is recommended that some effort be put forward in this endeavor.

Bibliography

1. Brouwer and Clemence. *Astrodynamics*. New York: McGraw-Hill, 1955.
2. Farquhar, R. W. *The Control and Use of Libration-Point Satellites*. Technical Report NASA TR R-346, Washington, DC: National Aeronautics and Space Administration, 1970.
3. Howell, K.C. and H.J. Pernicka. "A Station-Keeping Method for Libration Point Trajectories," *AIAA*, 713–723 (1990).
4. Howell, K.C. and H.J. Pernicka. "A Station-Keeping Method for Libration Point Trajectories," *Journal of Guidance and Control*, *16*:151–159 (1993).
5. Reid, Gary J. *Linear System Fundamentals (Continuous and Discrete, Classic and Modern)*. New York: Mcgraw-Hill, 1983.
6. Richardson, David L. "Halo Orbit Formulation for the ISEE-3 Mission," *Journal of Guidance and Control*, *3*:543–548 (1980).
7. Szebehely, Victor. *Theory of Orbits, The Restricted Problem of Three Bodies*. New York: Academic Press, 1967.
8. Wiesel, William E. *Spaceflight Dynamics*. New York: McGraw-Hill, 1989.
9. Wiesel, William E. *Advanced Astrodynamics*. WPAFB: Air Force Institute of Technology, 1992.
10. Wiesel, William E. and David J. Pohlen. "Canonical Floquet Theory," *Celestial Mechanics and Dynamical Astronomy* (1993).
11. Wiesel, William E. and W. Shelton. "Modal Control of an Unstable Periodic Orbit," *Journal of the Astronautical Sciences*, 63–76 (1983).

Vita

Douglas Hopper was born September 26, 1965 at Patrick AFB, Florida. He moved with his family to Kaysville, Utah in 1971 and graduated from Davis High School in 1983. In 1989 he graduated from Brigham Young University with a degree in Mechanical Engineering and was commissioned as an Air Force officer. He married the lovely Cindy Lee Lott in December of 1987 and they have a beautiful daughter named Roseanna. His first assignment was to Euro-NATO Joint Jet Pilot Training where he earned his pilot wings in December 1991. His next assignment was to the Air Force Institute of Technology.

Permanent address: 196 East 1050 North
Kaysville, Utah 84037

REPORT DOCUMENTATION PAGE

Form Approved
OMB No. 0704-0188

1. AGENCY USE ONLY (Leave blank)	2. REPORT DATE	3. REPORT TYPE AND DATES COVERED
	December 1993	Master's Thesis

4. TITLE AND SUBTITLE
Modal Control of a Satellite in an Unstable Periodic Orbit About the Earth-Sun Interior Lagrange Point

5. FUNDING NUMBERS

6. AUTHOR(S)
Douglas J Hopper, 1Lt, USAF

7. PERFORMING ORGANIZATION NAME(S) AND ADDRESS(ES)
Air Force Institute of Technology
Wright-Patterson AFB, OH 45433

8. PERFORMING ORGANIZATION REPORT NUMBER

9. SPONSORING/MONITORING AGENCY NAME(S) AND ADDRESS(ES)
Lt Col Salvatore Alfano
PL/VTA
Kirtland AFB, NM 87117-6008

10. SPONSORING/MONITORING AGENCY REPORT NUMBER
AFIT/GA/ENY/93D-3

11. SUPPLEMENTARY NOTES

12a. DISTRIBUTION/AVAILABILITY STATEMENT
Approved for public release; distribution unlimited

12b. DISTRIBUTION CODE

13. ABSTRACT *(Maximum 200 words)*

A periodic "halo" orbit which exists about the interior Lagrange point for the Earth-sun system was decomposed using Floquet theory into modal variables, which are dynamically decoupled subspaces for the six degree of freedom system. Modal control consisted of evaluating the diverging mode and maneuvering to counteract its divergence. In the unperturbed system, this was successful. Control costs were low, and the significance is that the controller did nothing to suppress modes that were oscillatory or converging. The effect of the moon's motion allowed the scheme to operate with reasonable control costs, but the effect of eccentricity caused divergence in spite of the controller.

14. SUBJECT TERMS		15. NUMBER OF PAGES
Floquet Theory	Modal Control	93
Periodic Orbits	ISEE - 3	16. PRICE CODE
Halo Orbits		

17. SECURITY CLASSIFICATION OF REPORT	18. SECURITY CLASSIFICATION OF THIS PAGE	19. SECURITY CLASSIFICATION OF ABSTRACT	20. LIMITATION OF ABSTRACT
Unclassified	Unclassified	Unclassified	UL